The influence of carbon nanotube coated-carbon fibers on thermal residual stresses of Multi-Scale hybrid composites: Analytical approach

The Influence of Carbon Nanotube Coated-Carbon Fibers on Thermal Residual Stresses of Multi-Scale Hybrid Composites: Analytical Approach

Reza Malekimoghadam[1,*], Ugo Icardi[1,], Seyyed Ahmad Hosseini[2]**

[1] Department of Mechanical and Aerospace Engineering, Politecnico di Torino, Corso Duca degli Abruzzi 24, 10129 Torino, Italy

[2] Institute of Materials Simulation, Friedrich-Alexander-Universität Erlangen-Nürnberg, Dr.-Mack-Str. 77, 90762 Fürth, Germany

Abstract

The effect of carbon nanotube (CNT) coated-carbon fibers on thermal residual stresses of multi-scale hybrid composites is assessed employing analytical approach. The model comprises carbon fiber, coating region and surrounding matrix, in which the coating region around core fiber encompasses CNTs and matrix. Considering three configurations of grown CNTs on the fiber surface including axially, radially and randomly oriented, the mechanical properties of various coating regions are acquired employing the Eshelby–Mori–Tanaka method in conjunction with an equivalent continuum approach. Utilizing the total energy minimization method, the closed-form solution of the thermal residual stresses of hybrid composite is obtained. The results disclose a noteworthy influence of CNT–coating on the reduction of interfacial stresses which precludes debonding at interface and attenuates the effect of thermal expansions mismatch between the carbon fiber and matrix. Furthermore, the results demonstrate that unlike radially oriented CNTs, the existence of axially and randomly oriented CNTs at the coating region has a remarkable diminishing effect on residual interfacial stresses. It is also shown that increasing the coating thickness leads to reduction of maximum interfacial stresses even at a constant CNT volume fraction. A close agreement exists between predicted outcomes by the proposed analytical approach and published data in the literature.

Keywords: Multi-Scale Hybrid Composite; CNT-Coating on Carbon Fiber; Analytical Approach; Residual Thermal Stress

[*] Corresponding Author. *Email Address:* reza.malekimoghadam@polito.it
** Corresponding Author. *Email Address:* ugo.icardi@polito.it

1. Introduction

Being cured or processed at elevated temperatures under pressure and/or in vacuum, the majority of composite materials attain their structural integrity [1–3]. In manufacturing or cooling processes, therefore, the residual stress is generated due to discrepancy in coefficient of thermal expansion (CTE) between the fiber and matrix. Hence, as a fundamental issue, fiber-matrix interfacial stresses induced by thermal conditions, remarkably affect the mechanical behavior and load transferring phenomenon in composite materials [4–7]. Thus, residual stress intrinsically emerges in almost all composite structures [8]. Multifarious methods have been accomplished in order to determine thermal residual stresses in the conventional fiber reinforced composites encompassing experimental investigations, elasticity solution and concentric cylinder theory in which thermal stresses are acquired for an infinitely long fiber surrounded by a matrix [9–13]. In the elasticity solution and concentric cylinder theory, the residual stresses are usually assumed to be independent of the fiber longitudinal direction [14]. In comparison with the aforementioned methods, the complementary energy method seems more advantageous because of (i) considering the stresses rather than the displacements as unknowns, (ii) introducing a better knowledge about residual stress distribution along the fiber direction and (iii) satisfying all boundary conditions especially at the fiber end [14].

Likewise, various finite element models (FEM) such as unit cell models of square and hexagonal arrays with different boundary conditions have been developed in order to obtain the thermoelastic behavior of composite structures [15,16]. Therefore, decreasing the fiber-matrix interfacial stress under thermal conditions plays a crucial role in augmenting the overall mechanical behavior through minimization of debonding. Consequently, CTE mismatch between the fiber and matrix is weakened by exploiting a suitable fiber coating [17,18].

Invoking nanomaterials as an efficient solution for coating the fibers in the conventional composites has recently been introduced. The breakthrough of carbon nanotubes (CNTs) and nanoparticles have burgeoned a novel research sphere among scientists because of their unique properties [19–24]. Chief among the nanomaterials, carbon nanotubes have been widely utilized in the field of fiber-reinforced composites with the aim of improving interfacial properties or adding new functionalities in which the CNTs' deposition on the fiber surfaces is one of the most promising techniques [25]. It has even been demonstrated that dispersion of a few portions of CNTs in a matrix remarkably increases the thermal and mechanical properties of composite

materials [26–28]. Owing to the superior characteristics of CNTs, multi-scale nano-engineered hybrid composites are being developed due to their outstanding behaviors in obviating cardinal drawbacks of conventional composites regarding interfacial and interlaminar properties by altering the fiber-matrix interface region [29]. Kundalwal and collaborators studied the thermomechanical properties and load transfer characteristics of the short fuzzy fiber reinforced composite utilizing shear lag model [30–32]. Chatzigeorgiou et al. [33-35] investigated the mechanical properties and introduced a homogenization approach of fuzzy fiber composites using concentric cylinder theory. Employing several analytical methods, the residual stresses in a conventional single fiber–matrix composite have been determined [36]. The analysis of thermal stresses in fibers of finite length embedded in a matrix is represented by Quek [37] employing a theoretical approach. The results revealed that the stress concentrations exist very close to the fiber ends which tend to enhance the likelihood of the fiber debonding due to mechanical loading and will influence the analysis of interfacial properties in fiber pull- and push-out tests. Mikata and Taya [38] investigated the stress field in a coated continuous fiber composite subjected to thermo-mechanical loadings, in which the results demonstrated that Ni-coating is advantageous over SiC-coating from the crack resistance point of view. Thermal stresses in the composite structures comprising fiber, pyrolytic-carbon coating and matrix were calculated by Honjo [39] making use of actual properties of carbon coating which are elastically and thermally cylindrically anisotropic.

The majority of the foregoing literature was devoted to residual stress analysis of conventional composite materials. Owing to the lack of a straight and efficient method for interfacial stress analysis of multi-scale hybrid composites, a micromechanics modeling approach in conjunction with energy minimization method is developed in the present work, capable of obtaining a closed form solution for such materials and remarkably decreasing the computation time with respect to finite element analysis. To this end, a CNT-coating region with different configurations including axial, radial, and random oriented CNT is taken into account around the carbon fiber. Utilizing the proposed method, the influence of CNT-coating on the fiber–matrix thermal residual stresses is assessed parametrically. Notably, the axial, hoop and radial stresses are considered in the energy formulation, for sake of achieving more accurate outcomes of the residual stress distribution.

2. Constitutive Modeling of CNT– Coated Carbon Fiber Hybrid Composite

There are different techniques for the deposition of CNTs on the surface of carbon fiber such as Chemical Vapor Deposition (CVD), electrophoresis, electrospray technique, etc., each of which has its advantages and limitations [40–42]. By systematically varying the catalyst concentration, catalyst pre-treatment time, and sample position within the tube furnace in CVD method, the key factors governing CNT morphology are achievable [43], i.e., CNTs could be grown in radial, axial or random orientations on the fiber surface [44,45]. The presence of CNTs forest on the surface of the fiber is delineated in Fig.1 invoking CVD and electrospray methods.

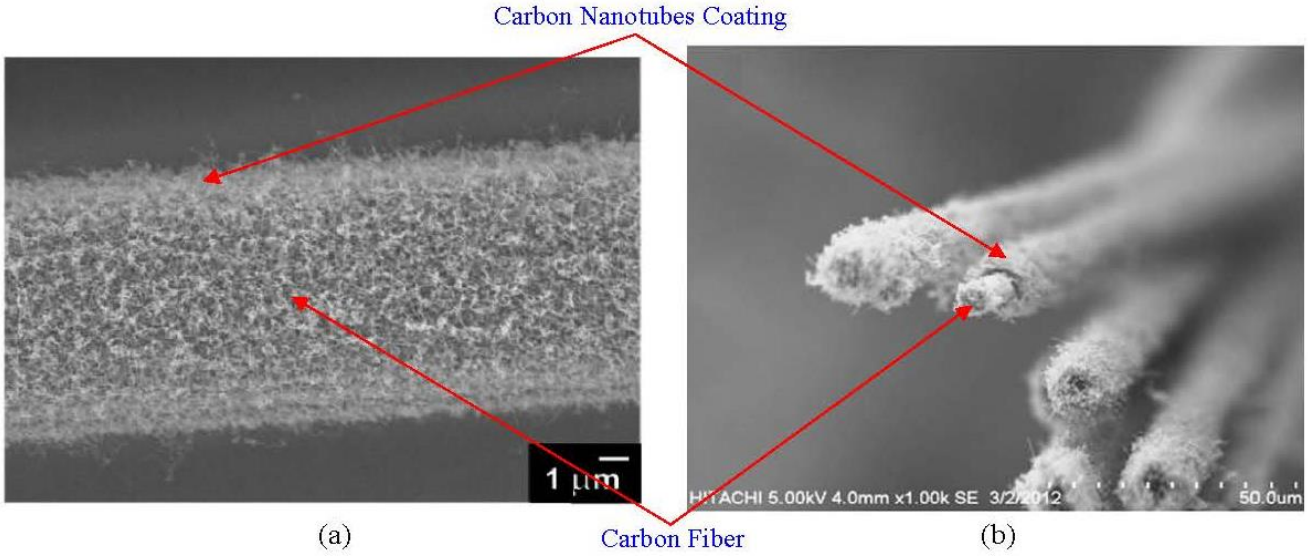

Fig. 1: Carbon fiber coated with CNT's forest (a) randomly oriented CNT's on the surface of the carbon fiber [45] (b) Growth of CNT's with uniform distribution on the fiber surface [46]

In order to scrutinize the influence of CNT– coating on the core fiber and the effect of its morphology on the residual stress of hybrid composite, we take into account CNTs with radial, axial and random orientations at the coating region. A constitutive modelling approach is adopted to analyze hybrid composites with such layouts through constructing a cylindrical representative volume element (RVE) considering three disparate CNT orientations which are depicted in Fig.2. It should be noted that the subfigures of Fig. 2 are schematics, and carbon nanotubes possess high aspect ratios (AR>350).

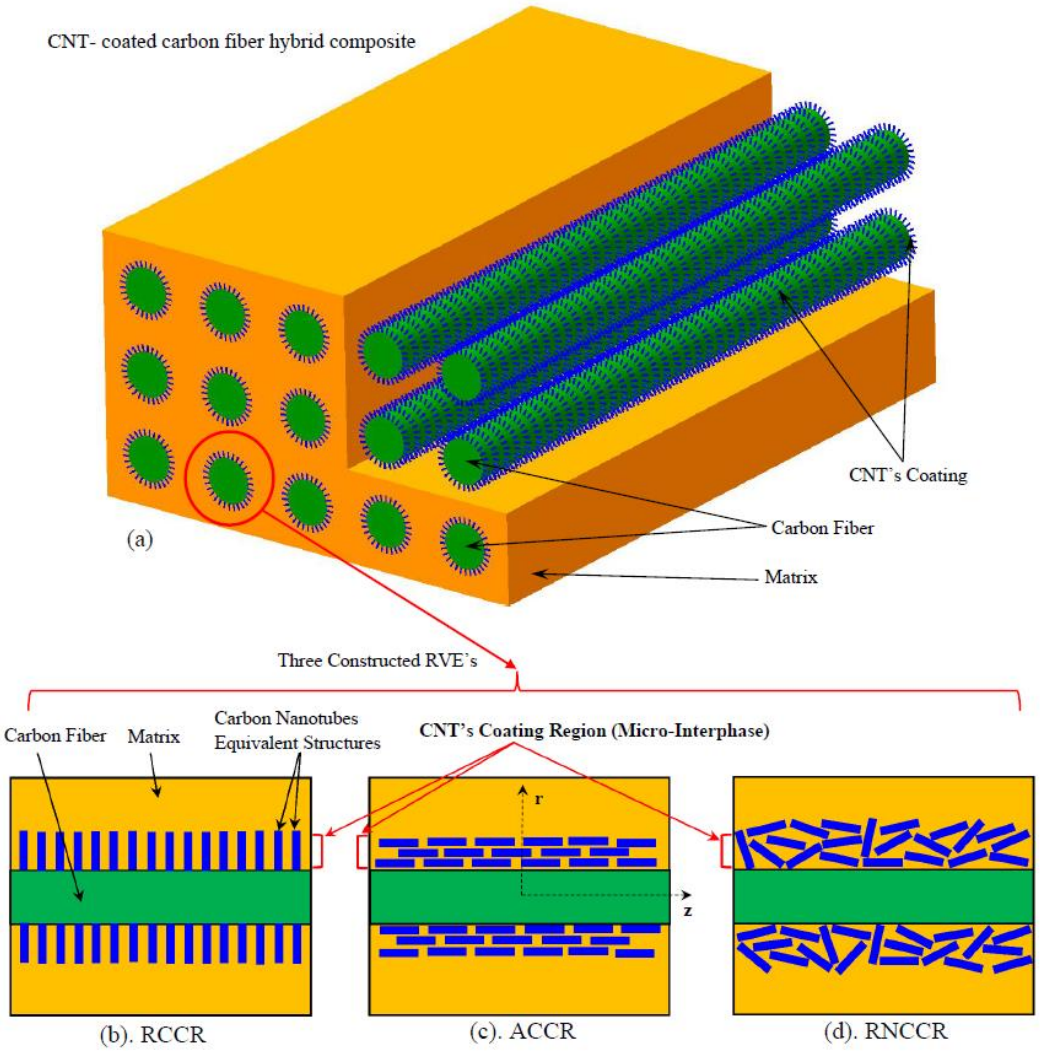

Fig. 2: Schematic illustration of RVE's including CNT coating configurations around core fiber (a) Multi- scale hybrid composite (b) With radially aligned CNTs (c) With axially aligned CNTs (d) With randomly oriented CNTs

The RVEs are established through three concentric cylinders consisting of carbon fiber, CNT-coating region (henceforth referred to as CCR) and surrounding matrix. The CCR could be considered as a nanocomposite itself, in which the constituents are matrix and CNTs. For sake of clarification, the consecutive modeling procedure in the present work is consolidated as a flowchart represented in Fig.3.

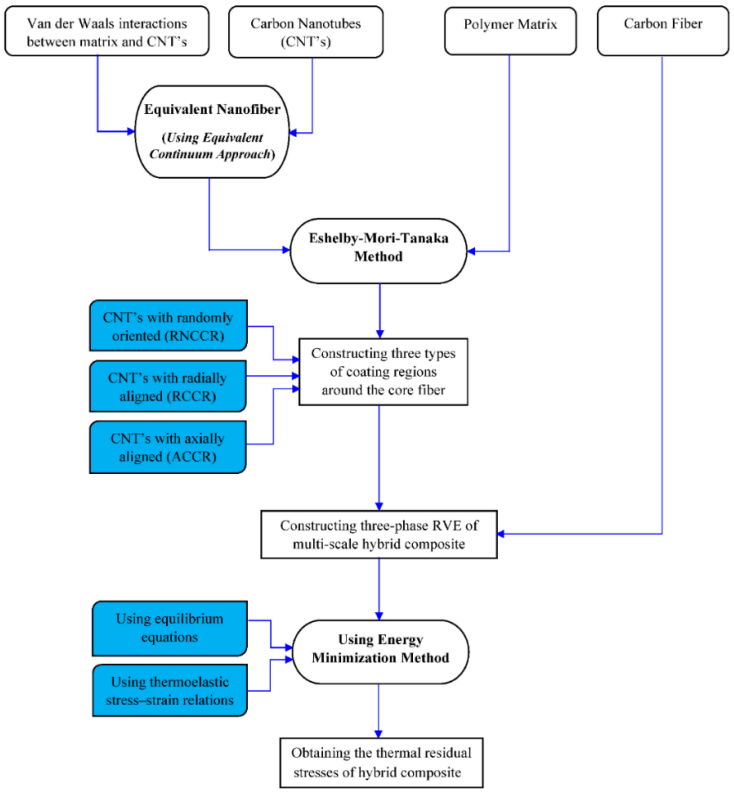

Fig. 3: Flowchart of obtaining residual stresses of CNT–coated carbon fiber hybrid composite

2.1. Modelling of Carbon Nanotube Structure

At nanoscale, CNTs behave as nano-reinforcement agents in the hybrid composites. The theoretical investigations in modeling CNT behaviors are classified in three categories comprising atomistic modeling, continuum modeling and nano-scale continuum modeling [47]. Concentrating on mechanical, buckling, vibrational and thermal properties, various approaches in the modeling of CNTs were rigorously reviewed and analyzed by Rafiee and Malekimoghadam [19]. Developing a finite element (FE) model of the CNT lattice structure by Li and Chou [48], each C–C bond of the CNT nanostructure is replaced with equivalent beam element in which the geometrical and mechanical properties of the beam element are obtained correlating the interatomic potential energies of molecular space to the strain energies of structural mechanics. Utilizing equivalent continuum modeling [49], the CNT structure with surrounding non-bonded interphase is represented as equivalent nanofiber (ENF) which is described in Fig.4 and the ENF mechanical properties can be acquired using multi-scale finite element modeling proposed by Rafiee and Malekimoghadam [50]. It should be mentioned that the governing interactions between

CNT and surrounding polymer are weakly non-bonded Van der Waals interactions. Conducting the multi-scale FE analysis, the non-bonded interphase region is simulated using nonlinear spring elements between CNT atoms and inner surface atoms of the polymer [50].

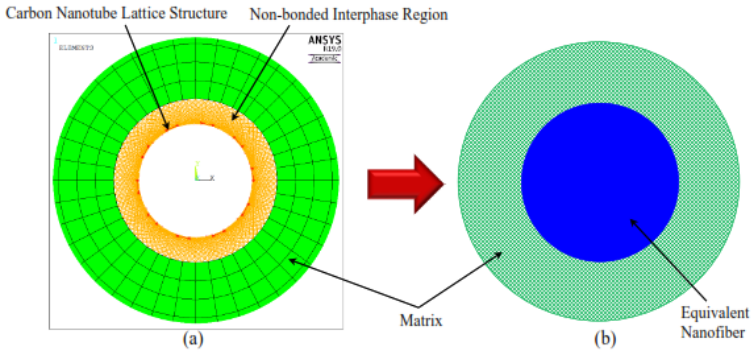

Fig. 4: Description of CNT equivalent modeling (a) FE multi-scale model (b) Equivalent nano-fiber

Finally, the mechanical properties of the CNT equivalent structure (ENF) are achieved [50] which are employed as input data for theoretical stresses analysis of hybrid composites in the present work.

Thus, the ENF accurately accounts for the structural properties relationships at the nanoscale and furnishes a bridge to the continuum model. The Hill's elastic moduli [51] of the reinforcing phase, which is CNT in the present work, are attained by equality of two following matrices of ENF [52]:

$$\mathbf{C}_{ENF} = \begin{pmatrix} n_{ENF} & l_{ENF} & l_{ENF} & 0 & 0 & 0 \\ l_{ENF} & k_{ENF}+m_{ENF} & k_{ENF}-m_{ENF} & 0 & 0 & 0 \\ l_{ENF} & k_{ENF}-m_{ENF} & k_{ENF}+m_{ENF} & 0 & 0 & 0 \\ 0 & 0 & 0 & p_{ENF} & 0 & 0 \\ 0 & 0 & 0 & 0 & m_{ENF} & 0 \\ 0 & 0 & 0 & 0 & 0 & p_{ENF} \end{pmatrix} \quad (1)$$

$$\mathbf{C}_{ENF} = \begin{pmatrix} \frac{1}{E_L} & -\frac{\upsilon_{TL}}{E_T} & -\frac{\upsilon_{ZL}}{E_Z} & 0 & 0 & 0 \\ -\frac{\upsilon_{LT}}{E_L} & \frac{1}{E_T} & -\frac{\upsilon_{ZT}}{E_Z} & 0 & 0 & 0 \\ -\frac{\upsilon_{LZ}}{E_L} & -\frac{\upsilon_{TZ}}{E_T} & \frac{1}{E_Z} & 0 & 0 & 0 \\ 0 & 0 & 0 & \frac{1}{G_{TZ}} & 0 & 0 \\ 0 & 0 & 0 & 0 & \frac{1}{G_{ZL}} & 0 \\ 0 & 0 & 0 & 0 & 0 & \frac{1}{G_{LT}} \end{pmatrix}^{-1} \quad (2)$$

Where k_{ENF}, l_{ENF}, m_{ENF}, n_{ENF}, and p_{ENF} parameters are the Hill's elastic moduli of equivalent nanofiber. Since CNT is considered as transversely isotropic material, the compliance matrix of Eq. (2) will contain five independent elastic parameters as E_L, E_T, G_{TZ}, υ_{TL}, υ_{TZ} which are derived from foregoing FEM and equivalent continuum modelling technique [50].

The material's properties of ENF for an armchair type single walled CNT with chiral index of (10, 10) are given in Table.1 [53,54].

Table 1: Mechanical Properties of Equivalent Nanofiber

Material	Longitudinal Young's modulus	Transverse Young's modulus	Transverse shear modulus	Poisson's ratio (υ_{LT})	Poisson's ratio (υ_{TZ})
Equivalent Nanofiber	649.12 [GPa]	11.27 [GPa]	5.13 [GPa]	0.284	0.14

2.2. Effective Elastic Properties of CNT– Coating Region (CCR)

The CCR which is also called micro-interphase region, encompasses grown CNTs, and polymer as a nanocomposite material surrounding carbon fiber. We take into account three configurations of CCR on the basis of the orientation of their constituent CNTs comprising radial, axial and random (henceforth referred to as RCCR, ACCR and RNCCR, respectively) as depicted in Fig.2b-d. It should be also noted that the CNTs in the RCCR model span the entire interphase thickness,

whereas in the ACCR configuration, they span the full length of the carbon fiber. In the RNCCR model, the CNTs span the full length in all orientations/ angles inside the coating region. In order to acquire the effective properties of fiber composites, multifarious micromechanics models comprising dilute concentration model based on the Eshelby's equivalent inclusion, the self-consistent model, Mori–Tanaka models, the Halpin–Tsai equations and shear lag models were reviewed by Tucker and Liang [55]. For predicting the effective properties of composites, the Mori–Tanaka model has been reported to be the efficient analytical technique [55]. Barral et al. [56] proposed an extension of the classical mean-field methods such as the Mori-Tanaka scheme combined with Transformation Field Analysis (TFA) accounting for a coated inclusion. The effectiveness of this new method is demonstrated through extensive numerical validation tests, including non-monotonic and non-proportional loading at different strain rates. Therefore, the Mori-Tanaka model [57] is employed in order to determine the effective elastic properties of CCR which is required as input data for residual stress analysis. It is worthwhile to note that the details of Mori-Tanaka schemes for different types of inclusions and multi-phase systems have been thoroughly explicated in the literature [58,59]. Employing the Mori-Tanaka method and taking into account the average over orientations of nanofibers, the stiffness tensor of CCR as a composite medium can be defined [60]. For a two-phase composite material, the effective stiffness tensor of CCR is expressed as [58,61]:

$$\mathbf{C}_{CCR} = \mathbf{C}_{\mathrm{m}} + V_{ENF} \left\{ (\mathbf{C}_{ENF} - \mathbf{C}_{m}) \ \mathbf{A}_{ENF} \right\} \left[V_{m}\mathbf{I} + V_{ENF} \left\{ \mathbf{A}_{ENF} \right\} \right]^{-1} \tag{3}$$

Where V_m and V_{ENF} indicate the volume fractions of matrix and CNT (effective nano-fiber), respectively, $\mathbf{I}$ is the fourth-order identity tensor, $\mathbf{C}_{\mathrm{CCR}}$, $\mathbf{C}_{\mathrm{m}}$ and $\mathbf{C}_{\mathrm{ENF}}$ are the stiffness tensors of CCR, matrix and equivalent nano-fiber (ENF), and $\mathbf{A}_{\mathrm{ENF}}$ denotes the dilute mechanical strain concentration tensor of ENF which is described as below. The Curly brackets {*} represent an average over all possible orientations.

$$\mathbf{A}_{ENF} = \left[\mathbf{I} + \mathbf{S} \ (\mathbf{C}_{m})^{-1} \ (\mathbf{C}_{ENF} - \mathbf{C}_{m}) \right]^{-1} \tag{4}$$

Where $\mathbf{S}$ is Eshelby's tensor [62] which is thoroughly elaborated by Mura [63] for various inclusions.

In view of the fact that the properties are different for each type of CNT coating, the stiffness matrices corresponding to RCCR, ACCR and RNCCR should be achieved separately. By obtaining the mechanical properties of three RVEs comprising different types of CNT coating (see Fig.2), the models are established for residual stress analysis.

It should be reaffirmed that the CNT structure treats as transversely isotropic material whereas the surrounding matrix behaves as an isotropic medium. Consequently, ACCR is transversely isotropic with an axis of symmetry along *z* direction (Fig.2-c). The stiffness matrix of ACCR in terms of Hill's moduli is expressed as following [61]:

$$\mathbf{C}_{ACCR}=\begin{pmatrix} k_{ACCR}+m_{ACCR} & l_{ACCR} & k_{ACCR}-m_{ACCR} & 0 & 0 & 0 \\ l_{ACCR} & n_{ACCR} & l_{ACCR} & 0 & 0 & 0 \\ k_{ACCR}-m_{ACCR} & l_{ACCR} & k_{ACCR}+m_{ACCR} & 0 & 0 & 0 \\ 0 & 0 & 0 & p_{ACCR} & 0 & 0 \\ 0 & 0 & 0 & 0 & m_{ACCR} & 0 \\ 0 & 0 & 0 & 0 & 0 & p_{ACCR} \end{pmatrix} \tag{5}$$

where *k*, *l*, *m*, *n*, and *p* are Hill's elastic moduli; *k* represents the plane-strain bulk modulus normal to the ENF direction, *n* denotes the uniaxial tension modulus along the ENF direction, *l* indicates the associated cross modulus, and *m* and *p* state the shear moduli in planes normal and parallel to the ENF direction, respectively. The non-vanishing components of the Eshelby tensor **S** are given as following for a straight ENF with circular cross section and sufficiently large aspect ratio along the z-direction [63]:

$$\begin{aligned} &S_{1111}=S_{3333}=\frac{5-4\upsilon_m}{8\,(1-\upsilon_m)}, \qquad S_{1122}=S_{3322}=\frac{\upsilon_m}{2\,(1-\upsilon_m)} \\ &S_{1133}=S_{3311}=\frac{4\upsilon_m-1}{8\,(1-\upsilon_m)}, \qquad S_{1212}=S_{2323}=\frac{1}{4}, \qquad S_{1313}=\frac{3-4\upsilon_m}{8\,(1-\upsilon_m)} \end{aligned} \tag{6}$$

Where υ_m is Poisson's ratio of the matrix. By substituting Eq. (6) into Eq. (4) the non-vanishing components of **A** are obtained accordingly:

$$A_{1111}=A_{3333}=-\frac{a_3}{a_1 a_2}\ ,\qquad A_{1133}=A_{3311}=\frac{a_4}{a_1 a_2}\ ,\qquad A_{2323}=\frac{E_m}{E_m+2\,p_{ENF}\ (1+\upsilon_m)}$$

$$A_{1122}=A_{3322}=\frac{l_{ENF}\ (1-\upsilon_m-2\upsilon_m{}^2)-E_m\,\upsilon_m}{a_1}\ ,\qquad A_{1313}=\frac{2\,E_m\,(1-\upsilon_m)}{a_2}\ ,\qquad A_{2222}=1 \tag{7}$$

Where E_m and υ_m are elastic modulus and Poisson's ratio of matrix and a_1, a_2, a_3, a_4 parameters are represented in Appendix A. The Hill's elastic moduli of CNTs are already obtained in section 2.1. By replacing the elements of tensor **A** from Eq. (7) into Eq. (3), the stiffness tensor of ACCR is achieved. In particular, the Hill's elastic moduli of foregoing CNT configuration are expressed as following [61]:

$$k_{ACCR}=\frac{E_m\left\{E_m V_m+2k_{ENF}\,(1+\upsilon_m)\,[1+V_{ENF}\,(1-2\upsilon_m)]\right\}}{2(1+\upsilon_m)\,[E_m\,(1+V_{ENF}-2\upsilon_m)+2V_m\,k_{ENF}\,(1-\upsilon_m-2\upsilon_m{}^2)]} \tag{8}$$

$$l_{ACCR}=\frac{E_m\left\{V_m\,\upsilon_m\,[E_m+2k_{ENF}\,(1+\upsilon_m)]+2V_{ENF}\,l_{ENF}\ (1-\upsilon_m{}^2)\right\}}{(1+\upsilon_m)\,[2V_m\,k_{ENF}\,(1-\upsilon_m-2\upsilon_m{}^2)+E_m\,(1+V_{ENF}-2\,\upsilon_m)]} \tag{9}$$

$$n_{ACCR}=\frac{E_m{}^2V_m\,(1+V_{ENF}-V_m\,\upsilon_m)+2V_m\,V_{ENF}\,(k_{ENF}\,n_{ENF}-l_{ENF}{}^2)(1+\upsilon_m)^2(1-2\upsilon_m)}{(1+\upsilon_m)\left\{2\,V_m\,k_{ENF}\,(1-\upsilon_m-2\upsilon_m{}^2)+E_m\,(1+V_{ENF}-2\upsilon_m)\right\}}+$$
$$\frac{E_m\,[2V_m{}^2k_{ENF}\,(1-\upsilon_m)+V_{ENF}\,n_{ENF}\,(1-2\upsilon_m+V_{ENF})-4V_m\,l_{ENF}\,\upsilon_m]}{2\,V_m\,k_{ENF}\,(1-\upsilon_m-2\upsilon_m{}^2)+E_m\,(1+V_{ENF}-2\upsilon_m)} \tag{10}$$

$$p_{ACCR}=\frac{E_m\,[E_m V_m+2(1+V_{ENF})\,p_{ENF}\,(1+\upsilon_m)]}{2\,(1+\upsilon_m)\,[E_m\,(1+V_{ENF})+2\,V_m\,p_{ENF}\,(1+\upsilon_m)]} \tag{11}$$

$$m_{ACCR}=\frac{E_m\,[E_m V_m+2\,m_{ENF}\,(1+\upsilon_m)(3+V_{ENF}-4\upsilon_m)]}{2(1+\upsilon_m)\left\{E_m\,[V_m+4V_{ENF}\,(1-\upsilon_m)]+2\,V_m\,m_{ENF}\,(3-\upsilon_m-4\upsilon_m{}^2)\right\}} \tag{12}$$

Where k_{ACCR}, l_{ACCR}, m_{ACCR}, n_{ACCR}, and p_{ACCR} are Hill's elastic moduli [54] of ACCR; k_{ACCR} is the plane-strain bulk modulus normal to the fiber direction, n_{ACCR} denotes the uniaxial tension modulus in the fiber direction (z- direction), l_{ACCR} indicates the associated cross modulus, and m_{ACCR} and p_{ACCR} state the shear moduli in planes normal and parallel to the fiber direction, respectively. Eventually, the longitudinal (E_Z, parallel to CNT direction) and transverse elastic moduli ($E_{r,\theta}$) of ACCR are declared in terms of Hill's elastic moduli as [60]:

$$(E_Z)_{ACCR} = n_{ACCR} - \frac{{l_{ACCR}}^2}{k_{ACCR}} \quad , \qquad (E_r)_{ACCR} = \frac{4\, m_{ACCR}\, (k_{ACCR}\, n_{ACCR} - {l_{ACCR}}^2)}{k_{ACCR}\, n_{ACCR} - {l_{ACCR}}^2 - m_{ACCR}\, n_{ACCR}} \tag{13}$$

On the other hand, the RCCR (Fig. 2b) is transversely isotropic with an axis of symmetry along *r* direction. Hence, after obtaining the mechanical properties of ACCR, the stiffness matrix of RCCR is also attained invoking below equation:

$$[\mathbf{C}_{RCCR}] = [\mathbf{T}]\,[\mathbf{C}_{ACCR}]\,[\mathbf{T}]^{T} \tag{14}$$

Where [**T**] denotes the transformation matrix which is given as following [64]:

$$\mathbf{T} = \begin{pmatrix} \cos^2\theta & \sin^2\theta & 0 & 0 & 0 & -\sin 2\theta \\ \sin^2\theta & \cos^2\theta & 0 & 0 & 0 & -\sin 2\theta \\ 0 & 0 & 1 & 0 & 0 & 0 \\ 0 & 0 & 0 & \cos\theta & -\sin\theta & 0 \\ 0 & 0 & 0 & \sin\theta & \cos\theta & 0 \\ -\sin\theta\cos\theta & \sin\theta\cos\theta & 0 & 0 & 0 & \cos^2\theta - \sin^2\theta \end{pmatrix} \tag{15}$$

For the case of RNCCR (Fig. 2d), the orientation distribution of CNTs could be characterized by a probability density function *p (α, β)* satisfying the below normalization condition [65]:

$$\int_0^{2\pi}\int_0^{\pi/2} p(\alpha,\beta)\sin\alpha \; \mathrm{d}\alpha\mathrm{d}\beta = 1 \tag{16}$$

Where α and β are two Euler angles which characterize the orientation of a straight CNT. If CNTs are randomly oriented, the density function is $p\ (\alpha, \beta) = 1/2\ \pi$. Thus, akin to Eq. (3), the effective modulus of the RNCCR can be stated as:

$$\mathbf{C}_{\mathrm{RNCCR}} = (V_m \mathbf{C}_{\mathrm{m}} + V_{ENF}\left\{\mathbf{C}_{ENF} : \mathbf{A}_{ENF}\right\}) : \left[V_m \mathbf{I} + V_{ENF}\left\{\mathbf{A}_{ENF}\right\}\right]^{-1} \tag{17}$$

It should be pointed out that if the CNTs are randomly distributed in the CCR, this region could be assumed as an isotropic material, and its bulk modulus *K* and shear modulus *G* are derived as [57]:

$$K_{RNCCR} = K_m + \frac{\mathrm{V}_{ENF}\ (\delta_{ENF} - 3K_m\,\alpha_{ENF})}{3\ (\mathrm{V}_m + \mathrm{V}_{ENF}\ \alpha_{ENF})}\ , \qquad G_{RNCCR} = G_m + \frac{\mathrm{V}_{ENF}\ (\eta_{ENF} - 2G_m\,\beta_{ENF})}{2(\mathrm{V}_m + \mathrm{V}_{ENF}\ \beta_{ENF})} \tag{18}$$

Where V_{ENF}, V_m, K_m and G_m are the volume fraction of nanofiber, volume fraction of matrix, bulk and shear moduli of the matrix, respectively. The parameters α_{ENF}, β_{ENF}, δ_{ENF} and η_{ENF} are given

in Appendix B. Finally, the effective Young's modulus (E) and Poisson's ratio (υ) of RNCCR are achieved as [60]:

$$E_{RNCCR} = \frac{9K_{RNCCR}\,G_{RNCCR}}{3K_{RNCCR}+G_{RNCCR}}, \qquad \upsilon_{RNCCR} = \frac{3K_{RNCCR}-2G_{RNCCR}}{6K_{RNCCR}+2G_{RNCCR}} \tag{19}$$

It is indicated that MATLAB R2018 platform has been utilized to calculate the stiffness matrices of CCRs (see Fig.2b-d) which are used as input data for subsequent section regarding interfacial residual stress analysis.

Since the CTE of CCR can be isotropic or anisotropic depending on the orientation of CNTs, a distinct CTE should be acquired for each CCR type. The effective CTEs of isotropic and anisotropic composite materials containing short and chopped fibers are derived by Marom and Weinberg [66] considering the fiber critical length. Making use of the shear-lag method, various investigations were carried out to develop expressions for the effect of the fiber aspect ratio (l/d) on the longitudinal (fiber-direction) CTE [67]. According to the foregoing investigation, the longitudinal CTE of CCR region can be express as:

$$(\alpha_{CCR})_L = \frac{K(E_{ENF})_L(\alpha_{ENF})_L V_{ENF} + E_m \alpha_m V_m}{K(E_{ENF})_L V_{ENF} + E_m V_m} \tag{20}$$

Where $(E_{ENF})_L$, $(\alpha_{ENF})_L$, V_{ENF}, E_m, α_m, and V_m are longitudinal Young's modulus of equivalent nanofiber (ENF), longitudinal CTE of ENF, volume fraction of ENF, Young's modulus of matrix, CTE of matrix and volume fraction of matrix, respectively. The fiber efficiency factor, K, is a function of the fiber length and orientation, given by [67]:

$$K = C\left(1-\frac{\tanh(\gamma l/d)}{\gamma l/d}\right)$$
$$\gamma = (2G_m/(E_{ENF})_L)^{1/2}\,(V_{ENF}{}^{-1/2}-1)^{-1/2} \tag{21}$$

The factor C =1 is employed to allow ENF orientation in ACCR or RCCR, whereas C=0.4 is used for RNCCR [67]. With regard to the transverse CTE of short fiber composite, an expression was presented [66] which can be rewritten for ACCR and RCCR as following:

$$(\alpha_{ACCR/RCCR})_T = (1+\upsilon_m)\alpha_m V_m + (1+\upsilon_{ENF})(\alpha_{ENF})_T V_{ENF} - (\alpha_{CCR})_L(\upsilon_{ENF} V_{ENF} + \upsilon_m V_m) \tag{22}$$

It is worthwhile to mention that the CTE of CNTs are extremely nonlinear with respect to the variation of temperature. The CTEs of various CNTs were predicted using molecular dynamics

(MDs) by Alamusi et al. [68], in which it was found that the axial CTEs vary nonlinearly with the temperature, however, they decrease linearly as the CNT diameter increases. Likewise, a set of empirical formulations was proposed for evaluating the CTEs of armchair and zigzag SWCNTs considering both temperature and diameter of CNT [68]. For the armchair single walled CNT with chiral index (10,10) which is employed in the current research, the below equations are given to acquire the axial and transverse CTEs of CNT [24, 32, 68]:

$$\begin{aligned}
&\text{Low Temperature } (1-301K)\\
&\alpha_L = (2D-1)\times10^{-10}T^4 - (2D-1)\times10^{-7}T^3 + (2D-5)\times10^{-5}T^2 - (30D-3)\times10^{-2}T\\
&\text{High Temperature } (301-901K)\\
&\alpha_L = -0.9D - (2\times10^{-8}T^3 - 6\times10^{-5}T^2 + 3\times10^{-2}T)
\end{aligned} \tag{23}$$

$$\alpha_T = 3.7601\times10^{-10}\Delta T^2 - 3.2189\times10^{-7}\Delta T - 3.2429\times10^{-8}$$

Where α_L, α_T are axial and transverse CTEs of CNT, D is the diameter of CNT, and T denotes the temperature.

3. Problem Formulation and Analytical Implementation

Achieving the mechanical properties of CCR considering three disparate CNT morphologies (three constructed RVEs) in the previous section, the interfacial residual stress analysis and parametric study of CNT– coated carbon fiber hybrid composite are carried out in this section. Hence, the selected RVE encompassing carbon fiber, CCR and surrounding matrix are introduced as three concentric cylinders and the cylindrical coordinate system (r, θ, z) is adopted in which the z-direction is coincident with the longitudinal axis of carbon fiber, forming an axisymmetric problem. It should be mentioned that carbon fiber is simulated as transversely isotropic material whereas the surrounding matrix is considered as a homogeneous isotropic material. It is worthwhile to emphasize that the CCR is considered as a transversely isotropic or isotropic material depending on the CNTs' configurations around carbon fiber.

Appropriate Airy stress functions [69] are used in order to define the stresses in the current research, satisfying the equilibrium equations. Fig.5 illustrates the RVE of multi-scale hybrid composite in which the R_m, R_{CCR}, R_f and L are matrix radius, CCR radius, carbon fiber radius and length of RVE, respectively.

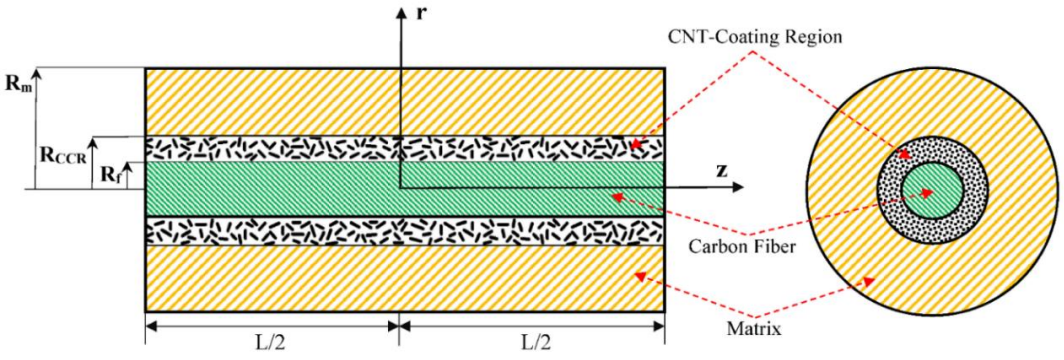

Fig. 5: RVE model of CNT- Coated fiber hybrid composite and corresponding coordinate system

3.1. Constructing the Stress Functions

In the cylindrical coordinate system, the equilibrium equation is expressed as [69]:

$$\frac{\partial \sigma_{zz}}{\partial z}+\frac{\partial \tau_{rz}}{\partial r}+\frac{\tau_{rz}}{r}=0 \tag{24}$$

$$\frac{\partial \sigma_{rr}}{\partial r}+\frac{\partial \tau_{rz}}{\partial z}+\frac{\sigma_{rr}-\sigma_{\theta\theta}}{r}=0 \tag{25}$$

The stress components in terms of Airy stress functions are stated as:

$$\sigma_{rr}=\frac{1}{r}\frac{\partial \varphi}{\partial r}+\frac{\partial^2 \varphi}{\partial z^2} \tag{26-a}$$

$$\sigma_{\theta\theta}=\frac{\partial^2 \varphi}{\partial z^2} \tag{26-b}$$

$$\sigma_{zz}=\frac{\partial^2 \varphi}{\partial r^2}+\frac{1}{r}\frac{\partial \varphi}{\partial r} \tag{26-c}$$

$$\tau_{rz}=-\frac{\partial^2 \varphi}{\partial r\,\partial z} \tag{26-d}$$

$$\tau_{z\theta}=\tau_{r\theta}=0 \tag{26-e}$$

In order to determine the axisymmetric state of stresses in the 3D problem of CNT-coated fiber hybrid composite, the Airy stress functions are assumed as following [70]:

$$\varphi_j(r,z) = f_q(r).g_q(z) \qquad q = 1,2,3 \quad ; \quad j = f, m, CCR \tag{27}$$

Where the subscripts f, CCR and m refer to the fiber, CNT-coating region and matrix, respectively. $f_q(r)$ and $g_q(z)$ are functions of radial and axial coordinates, respectively. Incorporating Eq. (27) in Equations (26-a)- (26-d), the stresses in the hybrid composite are attained accordingly:

$$\sigma_{rr}{}^{j} = \frac{1}{r}\frac{\mathrm{d}f_q(r)}{\partial r}g_q(z) + f_q(r)\frac{\mathrm{d}^2 g_q(z)}{\mathrm{d}z^2} \tag{28}$$

$$\sigma_{\theta\theta}{}^{j} = f_q(r)\frac{\mathrm{d}^2 g_q(z)}{\mathrm{d}z^2} \tag{29}$$

$$\sigma_{zz}{}^{j} = \left(\frac{\mathrm{d}^2 f_q(r)}{\mathrm{d}r^2} + \frac{1}{r}\frac{\mathrm{d}f_q(r)}{\mathrm{d}r}\right)g_q(z) \tag{30}$$

$$\tau_{rz}{}^{j} = -\frac{\mathrm{d}f_q(r)}{\mathrm{d}r}\frac{\mathrm{d}g_q(z)}{\mathrm{d}z} \tag{31}$$

It is worth mentioning that the number of unknown functions $f_1(r)$, $f_2(r)$ and $f_3(r)$ decreases by invoking boundary conditions of the stress-free state at the matrix surface as well as the stress continuity at the fiber–CCR interface and CCR–matrix interface along radial direction. Since the axial stress is assumed to be constant in radial direction (r) in each medium, the function $f_1(r)$, $f_2(r)$ and $f_3(r)$ can be described in terms of a constant B_q, while σ_{rr} and $\sigma_{\theta\theta}$ are still functions of r. Hence, by considering Eq. (30), the axial stresses in the fiber, matrix and CCR are given by [70]:

$$\sigma_{zz}{}^{f} = B_1.g_1(z) \tag{32}$$

$$\sigma_{zz}{}^{CCR} = B_2.g_2(z) \tag{33}$$

$$\sigma_{zz}{}^{m} = B_3.g_3(z) \tag{34}$$

Considering the equilibrium condition in the axial direction leads to [14]:

$$\sigma_{zz}{}^{f} V_f + \sigma_{zz}{}^{CCR} V_{CCR} + \sigma_{zz}{}^{m} V_m = 0 \tag{35}$$

Where V_f, V_m and V_{CCR} denote the volume fractions of fiber, matrix and CCR, respectively. Replacing Eqs (32)- (34) into Eq. (35) gives the below equation, whereby the three unknown functions $g_1(z)$, $g_2(z)$ and $g_3(z)$ are connected to each other that yields two unknown functions.

$$B_1 g_1(z) V_f + B_2 g_2(z) V_{CCR} + B_3 g_3(z) V_m = 0 \tag{36}$$

Utilizing the total complementary energy principle and Eq. (36), the two foregoing unknown functions will be determined and consequently the third one could be achieved by Eq. (36). Eventually, the axial, radial, shear and hoop stress components will be acquired in the constituents of the hybrid composite.

3.2. 3D Thermal Residual Stress Analysis of CNT-Coated Fiber Hybrid Composite

Following the aforementioned procedure and employing the complementary energy minimization, the thermal stresses induced in hybrid composite encompassing fiber, CCR and matrix are quantified and obtained subsequently.

3.2.1. Stress components in the fiber

Taking into account Eq. (32) and the first equilibrium equation, Eq. (24), the fiber shear stress is expressed as:

$$\tau_{rz}{}^{f} = -\frac{B_1 r}{2} \frac{\mathrm{d}g_1(z)}{\mathrm{d}z} \tag{37}$$

Due to finite value condition of stress in the core region, the fiber Airy stress function is only a function of z coordinate, and Eq. (26-a) and (26-b) can be stated as [14]:

$$\sigma_{rr}{}^{f} = \sigma_{\theta\theta}{}^{f} = \frac{\partial^2 \varphi}{\partial z^2} \tag{38}$$

Substituting Eq. (37) and Eq. (38) in the second equilibrium equation (Eq (25)), the radial and hoop stresses are given by:

$$\sigma_{rr}{}^{f} = \sigma_{\theta\theta}{}^{f} = \frac{B_1 r^2}{4} \frac{\mathrm{d}^2 g_1(z)}{\mathrm{d}z^2} + D_1(z) \tag{39}$$

3.2.2. Stress components in the CNT- coating region (CCR)

The stress components in CCR region are defined by substituting Eq. (33) in the equilibrium equations (Eq (24) and Eq. (25)):

$$\tau_{rz}^{CCR} = -\frac{1}{2r}\left\{B_1 {R_f}^2 \frac{\mathrm{d}g_1(z)}{\mathrm{d}z} + B_2(r^2 - {R_f}^2)\frac{\mathrm{d}g_2(z)}{\mathrm{d}z}\right\} \tag{40}$$

$$\sigma_{rr}^{CCR} = \sigma_{\theta\theta}^{CCR} = \frac{{R_f}^2}{2}\left\{B_1 \frac{\mathrm{d}^2 g_1(z)}{\mathrm{d}z^2} - B_2 \frac{\mathrm{d}^2 g_2(z)}{\mathrm{d}z^2}\right\}\ln r + B_2 \frac{r^2}{4}\frac{\mathrm{d}^2 g_2(z)}{\mathrm{d}z^2} + D_2(z) \tag{41}$$

3.2.3. Stress components in the matrix

Inserting Eq. (32) and Eq. (33) into Eq. (35) yields the axial stress in the surrounding matrix as following:

$$\sigma_{zz}^{m} = -\left\{B_1 g_1(z)\frac{V_f}{V_m} + B_2 g_2(z)\frac{V_{CCR}}{V_m}\right\} \tag{42}$$

Replacing the matrix axial stress in the equilibrium equations leads to:

$$\tau_{rz}^{m} = -\frac{B_1}{2r}\left\{{R_f}^2 - (r^2 - {R_{CCR}}^2)\frac{V_f}{V_m}\right\}\frac{\mathrm{d}g_1(z)}{\mathrm{d}z} - \frac{B_2}{2r}\left\{({R_{CCR}}^2 - {R_f}^2) - (r^2 - {R_{CCR}}^2)\frac{V_{CCR}}{V_m}\right\}\frac{\mathrm{d}g_2(z)}{\mathrm{d}z} \tag{43}$$

$$\begin{aligned}\sigma_{rr}^{m} = \sigma_{\theta\theta}^{m} = \frac{B_1}{4}&\left\{2{R_f}^2 lnr - (r^2 - 2{R_{CCR}}^2\ln r)\frac{V_f}{V_m}\right\}\frac{\mathrm{d}^2 g_1(z)}{\mathrm{d}z^2} + \\ &\frac{B_2}{4}\left\{2({R_{CCR}}^2 - {R_f}^2)lnr - (r^2 - 2{R_{CCR}}^2\ln r)\frac{V_{CCR}}{V_m}\right\}\frac{\mathrm{d}^2 g_2(z)}{\mathrm{d}z^2} + D_3(z)\end{aligned} \tag{44}$$

3.2.4. Boundary Conditions

The half of RVE length (from z=0 to z= L/2) is utilized due to the symmetry of the model. Thus, the free surface conditions [37] engender zero axial and shear stresses at end of the fiber as following:

$$\begin{aligned}&\rightarrow \quad g_q(0) = 1, && q = 1, 2\\ &\rightarrow \quad g_q'(0) = \frac{\mathrm{d}g_q(0)}{\mathrm{d}z} = 0,\\ &\rightarrow \quad g_q(L/2) = 0,\\ &\rightarrow \quad g_q'(L/2) = \frac{\mathrm{d}g_q(L/2)}{\mathrm{d}z} = 0,\end{aligned} \tag{45}$$

It is worth mentioning that the radial stress at the outermost surfaces of the polymer is zero and it also must be continuous across the fiber–CCR and CCR–matrix interfaces [70, 71]:

$$\sigma_{rr}{}^{m} = 0 \quad at \quad r = R_m, \qquad -\frac{L}{2} < z < \frac{L}{2} \tag{46}$$

$$\begin{aligned} &\sigma_{rr}{}^{f} = \sigma_{rr}{}^{CCR} \quad at \quad r = R_f, \qquad -\frac{L}{2} < z < \frac{L}{2} \\ &\sigma_{rr}{}^{CCR} = \sigma_{rr}{}^{m} \quad at \quad r = R_{CCR}, \qquad -\frac{L}{2} < z < \frac{L}{2} \end{aligned} \qquad \text{Continuity Conditions} \tag{47}$$

Satisfying the conditions of Eqs. (46) and (47), the unknown functions $D_1(z)$, $D_2(z)$ and $D_3(z)$ in Eqs. (39), (41) and (44) are obtained as follows:

$$\begin{aligned} D_1 = &-\frac{B_1}{4}\frac{d^2 g_1(z)}{dz^2}\left[2R_f^2 \ln R_m - (R_m^2 - 2R_{CCR}^2 \ln R_m)\frac{V_f}{V_m} + (R_{CCR}^2 - 2R_{CCR}^2 \ln R_{CCR})\frac{V_f}{V_m} - R_f^2 \ln R_f\right] \\ &-\frac{B_2}{4}\frac{d^2 g_2(z)}{dz^2}\left[2(R_{CCR}^2 - R_f^2)\ln R_m - (R_m^2 - 2R_{CCR}^2 \ln R_m)\frac{V_{CCR}}{V_m} - 2(R_{CCR}^2 - R_f^2)\ln R_{CCR}\right. \\ &\left. + (R_{CCR}^2 - 2R_{CCR}^2 \ln R_{CCR})\frac{V_{CCR}}{V_m} - 2R_f^2 \ln R_{CCR} + R_{CCR}^2 + 2R_f^2 \ln R_f - R_f^2\right] \end{aligned} \tag{48}$$

$$\begin{aligned} D_2 = &-\frac{B_1}{4}\frac{d^2 g_1(z)}{dz^2}\left[2R_f^2 \ln R_m - (R_m^2 - 2R_{CCR}^2 \ln R_m)\frac{V_f}{V_m} + (R_{CCR}^2 - 2R_{CCR}^2 \ln R_{CCR})\frac{V_f}{V_m}\right] \\ &-\frac{B_2}{4}\frac{d^2 g_2(z)}{dz^2}\left[2(R_{CCR}^2 - R_f^2)\ln R_m - (R_m^2 - 2R_{CCR}^2 \ln R_m)\frac{V_{CCR}}{V_m} - 2(R_{CCR}^2 - R_f^2)\ln R_{CCR}\right. \\ &\left. + (R_{CCR}^2 - 2R_{CCR}^2 \ln R_{CCR})\frac{V_{CCR}}{V_m} - 2R_f^2 \ln R_{CCR} + R_{CCR}^2\right] \end{aligned} \tag{49}$$

$$\begin{aligned} D_3 = &-\frac{B_1}{4}\frac{d^2 g_1(z)}{dz^2}\left[2R_f^2 \ln R_m - (R_m^2 - 2R_{CCR}^2 \ln R_m)\frac{V_f}{V_m}\right] - \frac{B_2}{4}\frac{d^2 g_2(z)}{dz^2}\left[2(R_{CCR}^2 - R_f^2)\ln R_m\right. \\ &\left. - (R_m^2 - 2R_{CCR}^2 \ln R_m)\frac{V_{CCR}}{V_m}\right] \end{aligned} \tag{50}$$

3.2.5. Thermo- elastic equations

The thermoelastic stress–strain relations of the hybrid composite are expressed as:

$$\varepsilon_{zz}{}^{j} = \frac{1}{(E^{j})_{z}} [\sigma_{zz}{}^{j} - \upsilon_{L}{}^{j}(\sigma_{rr}{}^{j} + \sigma_{\theta\theta}{}^{j})] + \alpha_{L}{}^{j}\Delta T \tag{51}$$

$$\varepsilon_{rr}{}^{j} = \frac{1}{(E^{j})_{r}} [\sigma_{rr}{}^{j} - \upsilon_{T}{}^{j}(\sigma_{zz}{}^{j} + \sigma_{\theta\theta}{}^{j})] + \alpha_{T}{}^{j}\Delta T \tag{52}$$

$$\varepsilon_{\theta\theta}{}^{j} = \frac{1}{(E^{j})_{\theta}} [\sigma_{\theta\theta}{}^{j} - \upsilon_{T}{}^{j}(\sigma_{zz}{}^{j} + \sigma_{rr}{}^{j})] + \alpha_{T}{}^{j}\Delta T \tag{53}$$

$$\gamma_{rz}{}^{j} = \frac{\tau_{rz}{}^{j}}{G_{rz}{}^{j}} \tag{54}$$

Where superscript j indicates the hybrid composite constituents, i.e., fiber, CCR and matrix. E_z, E_r, G, υ_L, υ_T, α_L and α_T represent the longitudinal elastic modulus, transverse elastic modulus, shear modulus, longitudinal Poisson's ratio, transverse Poisson's ratio, longitudinal CTE and transverse CTE, respectively.

3.2.6. Energy minimization

The two unknown constants B_1, B_2 and two unknown functions $g_1(z)$ and $g_2(z)$ will be acquired by minimizing the total complementary energy of the multi-scale hybrid composite (HC). The total complementary energy is described as:

$$\Pi_{HC} = U_{HC} + V_{HC} \tag{55}$$

where U_{HC} and V_{HC} are the complementary strain energy and the complementary potential energy of hybrid composite, respectively. Since the hybrid composite is free of any tractions and external loads, V_{HC}=0. Consequently, the total complementary energy can be stated as:

$$\begin{aligned} \Pi_{HC} &= \iiint_{V_t} \frac{1}{2} \boldsymbol{\tau}_{ij}\, \boldsymbol{\varepsilon}_{ij}\, \mathrm{d}v \qquad\qquad (t = f, m, CCR) \\ &= \iiint_{V_t} \left(\frac{1}{2}\, \sigma_{zz}{}^{t} \varepsilon_{zz}{}^{t} + \frac{1}{2}\, \sigma_{rr}{}^{t} \varepsilon_{rr}{}^{t} + \frac{1}{2}\, \sigma_{\theta\theta}{}^{t} \varepsilon_{\theta\theta}{}^{t} + \tau_{rz}{}^{t} \varepsilon_{rz}{}^{t} \right) r\, \mathrm{d}r\, \mathrm{d}\theta\, \mathrm{d}z \end{aligned} \tag{56}$$

It should be mentioned that for axial symmetry, $\tau_{r\theta} = \tau_{\theta z} = 0$. The total energy of hybrid composite expressed in Eq. (56) has 12 terms consisting of axial, radial, hoop and shear stresses for all three domains as fiber, CCR and matrix. The integrations of axial, radial and shear terms of the CCR in

Eq. (56) are calculated in the Appendix C. For sake of conciseness, the integration of matrix and fiber phases are excluded since they possess the same procedures to CCR.

Having obtained the function $D_1(z)$, $D_2(z)$ and $D_3(z)$ by satisfying boundary and continuity conditions, they are then embedded into Eqs. (39), (41) and (44) in order to achieve the radial and tangential stresses.

Eventually, by incorporating Eqs. (32), (33), (37), (39) and (40)- (44) and the thermo-elastic Eqs. (51)- (54) into Eq. (56), the total complementary energy is established.

Implementing the integration of total complementary energy with respect to r and θ engenders an integral function in terms of two unknown functions $g_1(z)$ and $g_2(z)$ and their derivatives, and two unknown constants B_1 and B_2 [14]:

$$\Pi_{HC} = 2\pi \int_{-L/2}^{L/2} F\,[B_1, B_2, g_1(z), g_1'(z), g_1''(z), g_2(z), g_2'(z), g_2''(z)]\mathrm{d}z \tag{57}$$

Invoking the calculus of variation, the Euler–Lagrange equation is expressed as:

$$\begin{aligned} &-\frac{\mathrm{d}^2}{\mathrm{d}z^2}\left(\frac{\partial F}{\partial g_1''(z)}\right)+\frac{\mathrm{d}}{\mathrm{d}z}\left(\frac{\partial F}{\partial g_1'(z)}\right)-\frac{\partial F}{\partial g_1(z)}=0 \\ &-\frac{\mathrm{d}^2}{\mathrm{d}z^2}\left(\frac{\partial F}{\partial g_2''(z)}\right)+\frac{\mathrm{d}}{\mathrm{d}z}\left(\frac{\partial F}{\partial g_2'(z)}\right)-\frac{\partial F}{\partial g_2(z)}=0 \end{aligned} \tag{58}$$

After inserting F from Eq. (57) into Eq. (58), we have obtained the two coupled fourth-order ordinary differential equations of multi-scale hybrid composites with respect to $g_1(z)$ and $g_2(z)$ which are:

$$\begin{cases} B_1^2 A_1\left(\frac{\mathrm{d}^4 g_1(z)}{\mathrm{d}z^4}\right)+B_1^2 A_2\left(\frac{\mathrm{d}^2 g_1(z)}{\mathrm{d}z^2}\right)+B_1^2 A_3 g_1(z)+\left[B_2 B_1 A_4\left(\frac{\mathrm{d}^4 g_2(z)}{\mathrm{d}z^4}\right)+B_2 B_1 A_5\left(\frac{\mathrm{d}^2 g_2(z)}{\mathrm{d}z^2}\right)+B_2 B_1 A_6 g_2(z)+B_1 A_7\right]=0 \\ B_2^2 A_8\left(\frac{\mathrm{d}^4 g_2(z)}{\mathrm{d}z^4}\right)+B_2^2 A_9\left(\frac{\mathrm{d}^2 g_2(z)}{\mathrm{d}z^2}\right)+B_2^2 A_{10} g_2(z)+\left[B_2 B_1 A_{11}\left(\frac{\mathrm{d}^4 g_1(z)}{\mathrm{d}z^4}\right)+B_2 B_1 A_{12}\left(\frac{\mathrm{d}^2 g_1(z)}{\mathrm{d}z^2}\right)+B_2 B_1 A_6 g_1(z)+B_2 A_{13}\right]=0 \end{cases} \tag{59}$$

Where the coefficients A_1-A_{13} signify the functions of materials and geometry properties of CNT–coated CF hybrid composite which are lengthy expressions for presenting in the article and are available on request. Due to the complexity, the mathematical software Maple 2019 is utilized in order to solve the equations. By solving the aforementioned equations, eight unknown constants emerge in $g_1(z)$ and $g_2(z)$, which are obtained by applying the boundary condition expressed in the

section 3.2.4 (eight boundary conditions). However, two unknown constants B_1 and B_2 still appear in Eq. (59). By replacing the solutions achieved for $g_1(z)$ and $g_2(z)$ and their derivatives into Eq. (57) and integrating with respect to z, the total complementary energy is attained in terms of B_1 and B_2. Through minimizing this equation, a set of linear equations is established and the unknown constants B_1 and B_1 are finally defined.

$$\frac{d\Pi_{HC}}{dB_1}=0$$
$$\frac{d\Pi_{HC}}{dB_2}=0 \qquad (60)$$

By substituting the $g_1(z)$, $g_2(z)$, B_1 and B_2 into equations (37) – (44), the distributions of the interfacial thermal residual stresses are achieved in the constituents of the hybrid composite including fiber, CCR and matrix. The present work is validated with close agreement by multi-scale finite element modeling (see Fig.6) proposed by Malekimoghadam and Icardi [5] for randomly oriented CNTs as displayed in Fig.7.

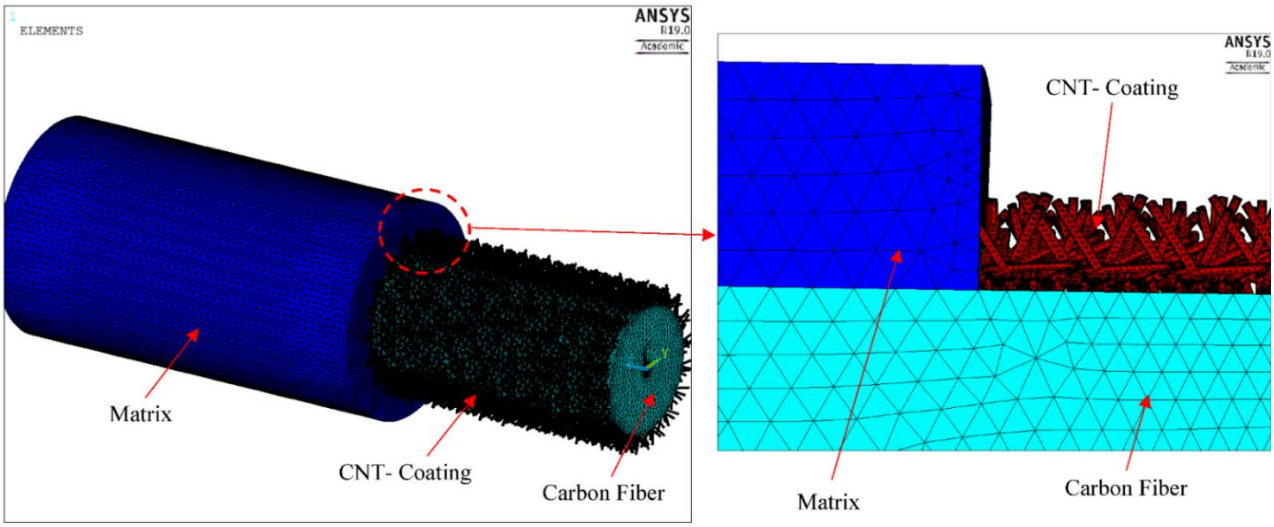

Fig. 6: Multi-scale Finite element model (a) CNT–Carbon Fiber hybrid composite (b) Cut-view

4. Result and Discussion

In this section the influence of CNTs coating on the carbon fiber surface is assessed on the distributions of thermal residual interfacial stresses. Subsequently, a parametric study is conducted based on the different effective parameters at each scale such as CNTs' orientations, CNT volume

fraction and coating thickness. Having acquired the stresses distributions, the results are then compared with the residual stress in the conventional composites implemented by Quek [37] and verified with multi-scale finite element modeling [5]. The properties of carbon fiber [39,72] and polymer matrix [73] are presented in Table.2. It should be mentioned the radius of the carbon fiber is considered as 3.5 μm [38].

Table 2: Elastic Properties of Carbon Fiber and Polymer Matrix

Material	E_z [GPa]	E_x, E_y [GPa]	G_{xz}, G_{yz} [GPa]	G_{xy} [GPa]	υ_{xz}	υ_{xy}	CTE_z [10^{-6}/°C]	CTE_r [10^{-6}/°C]
Carbon Fiber	230	28.7	25	7	0.3	0.42	1.1	6.8
Epoxy	4.20	-	-	-	0.31	-	60	-

Given that the maximum interfacial stresses play the most crucial roles in debonding between fiber and matrix and failure of composite structures, applying the CNTs coating on the core fiber will reduce the interfacial stresses. Introducing the CNTs at the coating region represents relatively small and shallow debonding areas at the connection between the fiber and the CCR than the debonding area at fiber-matrix interface in the composite without fiber coating [41]. Furthermore, the above-mentioned issue indicates that the CNTs have a higher adhesion force with the matrix and deboning will take place between fiber and coating region which reveals that fracture mode of carbon fiber–matrix composites is affected by CNT deposition [41]. The distributions of thermal residual stresses of multi-scale hybrid composite for RNCCR are represented in Fig.7. It should be mentioned that in all figures the radial and axial interfacial residual stresses are obtained at the fiber-CCR interface. Furthermore, the stresses are normalized by the interfacial stresses of fiber-matrix composite (without coating) developed by Quek [37]. The normalized length in all figures is acquired by (z/l), in which z is the longitudinal position along the fiber axis and l denotes the length of fiber. It can be inferred from Fig.7 that growth of solely 1wt.% of randomly oriented CNTs on the surface of carbon fiber markedly reduces the residual interfacial shear and radial stresses by 27% and 21%, respectively, assuming the temperature variation (ΔT) of 50 K and coating thickness of 900 nm. It is also worth mentioning that by increasing the CNTs content in the CCR by 2 wt.%, the coating stiffness increases which leads to reduction of interfacial stresses. According to experimental investigation [13], about 21% reduction of the maximum interfacial

stress was acquired by adding a small portion of multi-walled CNTs. It should be noted that the maximum interfacial shear and radial stresses in the finite element modeling are 5.8% and 4.9% higher than the analytical approach proposed in the present work, respectively. The foregoing issue is ascribed to the direct presence of debonding damage between CNTs and matrix in the FEM work, whereas in the present work the effect of interphase is taken into account indirectly, using the equivalent continuum approach introduced in section 2.1. More details of the influence of deboning damages on the interfacial stresses can be achieved from Ref [5]. Likewise, the result of the residual interfacial shear and radial stresses of conventional fiber reinforced composites considering perfect bond between fiber and matrix, performed by Quek [37], is inserted in Fig. 6 as the upper bound criteria. As expected, the maximum value of interfacial shear and radial stresses occur in contiguity of the fiber end and exactly at the fiber end, respectively.

In addition to the position of maximum stress, the amount of peak shear stress is of great importance since the debonding between fiber and matrix will ensue if the maximum interfacial stress transgresses the interfacial strength. Consequently, due to coating the core fiber with nanomaterials, the advanced multi-scale hybrid composites will represent strikingly lower interfacial residual thermal stresses which improve the performance of composite structures under different temperature gradient conditions.

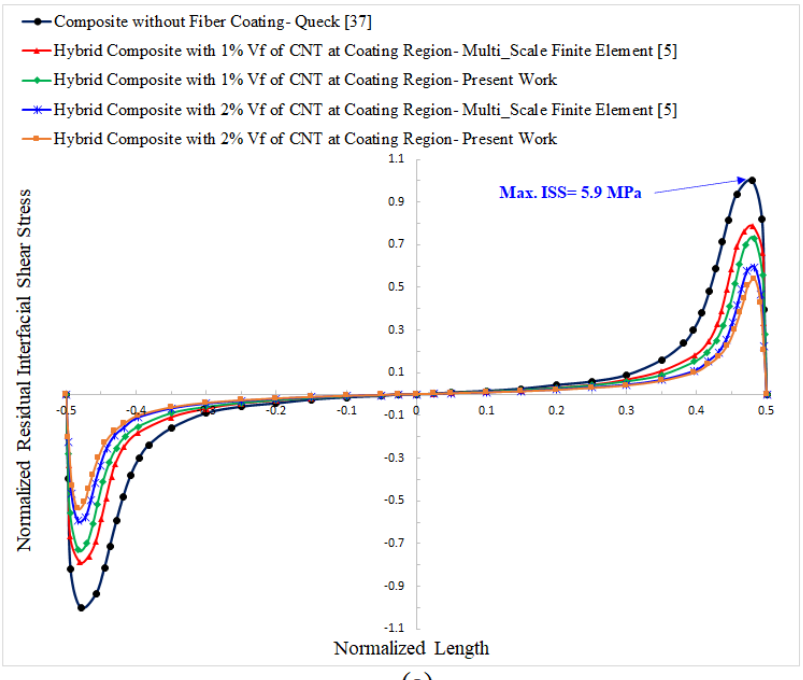

(a)

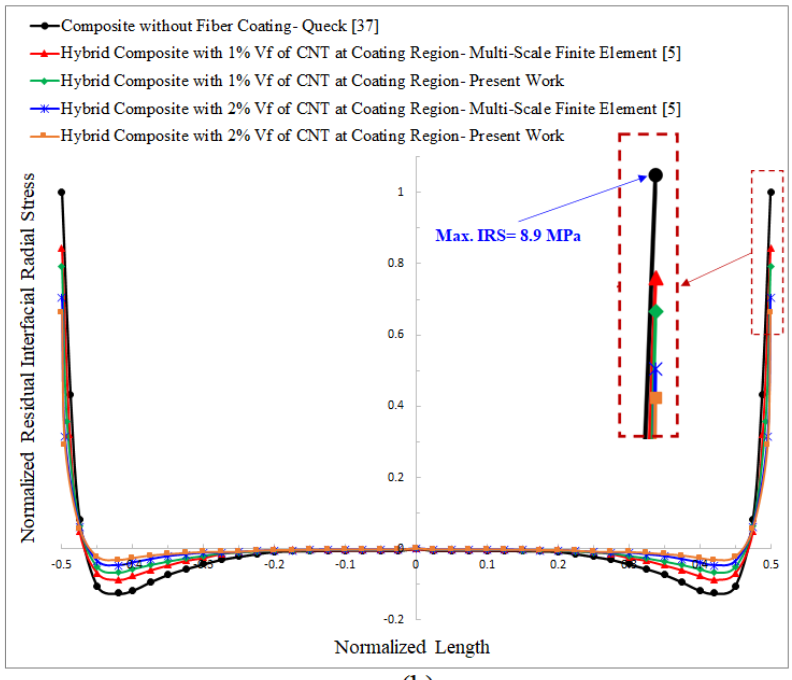

(b)

Fig. 7: Distribution of thermal residual interfacial stresses of hybrid composite, with coating thickness of 900 nm (a) Shear stress (b) Radial stress

Including various configurations of CNTs at the coating region, namely, RCCR, RNCCR and ACCR, the thermal residual interfacial stresses of CNT–CF multi-scale hybrid composite are depicted in Fig.8 considering a coating thickness of 900 nm and ΔT= 50 K. The results disclose that the configuration of CNTs at the coating region not only affects the mechanical properties of the coating medium, but also leads to significant difference of interfacial stresses which consequently varies the load transferring between fiber and matrix.

As it is described, ACCR and RCCR demonstrate the highest and lowest contribution towards reduction of thermal residual interfacial stresses, respectively, while the multi-scale hybrid composite with RNCCR represents reinforcement magnitude between the two aforementioned configurations. It is noteworthy to indicate that the models containing ACCR can make a valuable contribution to the reduction of residual interfacial shear and radial stresses under thermal loading. Furthermore, by introducing RCCR and RNCCR on the fiber surface, the residual interfacial shear stresses decrease by 7% and 27%, respectively, in comparison with a composite without fiber coating. Thus, the multi-scale hybrid composite comprising RNCCR exhibits much improved interfacial properties than that with RCCR which reveals the slight influence of radially grown CNTs at coating region on the interfacial properties. Consequently, it can be postulated that by aligning the CNTs at coating region along the axial direction of core fiber, the minimum interfacial stresses can be achieved which weaken the effect of mismatch between the CTEs of fiber and matrix under thermal loading. Interestingly, by employing the single- fiber fragmentation test, Sager et. al [74] demonstrated that randomly oriented and radially oriented MWCNT coated fibers augment the interfacial shear strength by 71% and 11%, respectively, which reaffirm the pronounced effect of randomly oriented CNTs on the fiber coating.

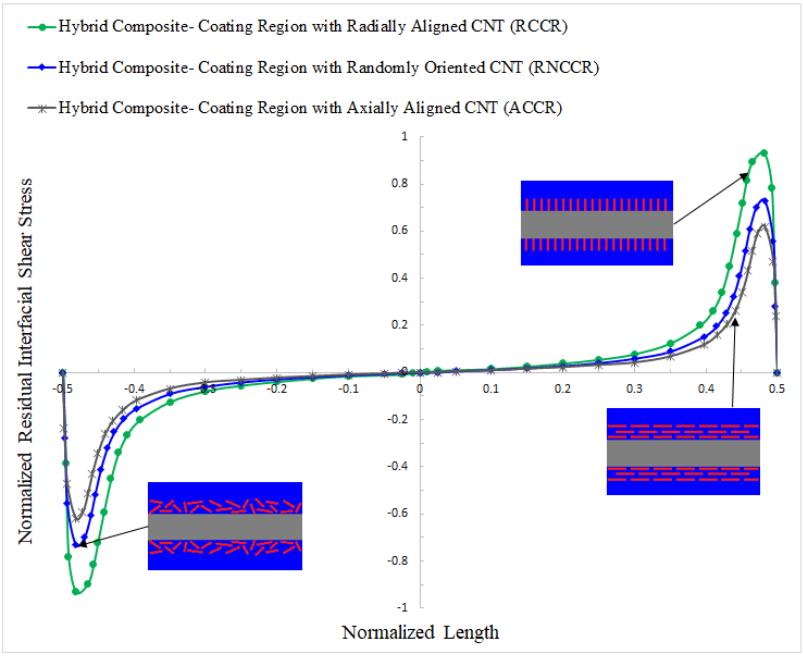

(a)

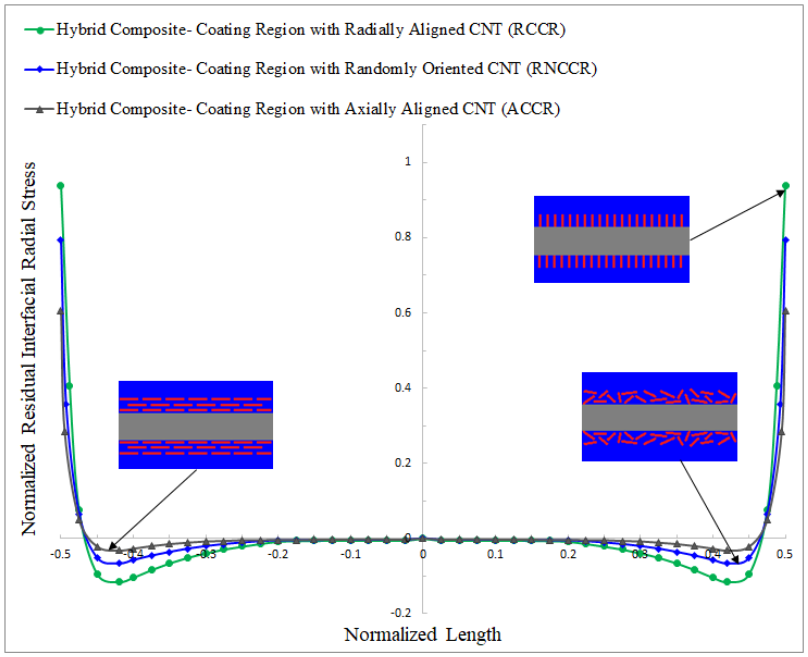

(b)

Fig. 8: Distribution of thermal residual interfacial stresses of hybrid composite considering different CNT's orientations at coating region(a) Shear stress (b) Radial stress

It should be asserted that two methods could be considered regarding the production of multi-scale hybrid composites, namely mixing CNTs entirely throughout the matrix and depositing CNTs on core fibers (fiber coating). Taking into account the similar CNT volume fraction, the former makes negligible influence on reduction of the interfacial stresses between fiber and matrix, while the latter provides graded interphase (coating region) around core fiber with diminishing effect on the interfacial stresses [5,75,76]. It should be mentioned, if the graded interphase is considered for improving the interfacial properties, gradual gradation will occur instead of steep gradation which is the key issue in attenuating CTE mismatch between fiber and matrix.

As one of the crucial parameters in the fiber coating, the effect of coating thickness on the residual interfacial stresses and fiber axial stress is displayed in Fig.9 for ΔT= 100 K. Different coating thicknesses around core fiber in the range of 300-1000 nm are usually obtained [44,45]. However, the thickness of CNT–coating around carbon fiber is demonstrated to be a function of CNT growth time and temperature in CVD technique, and it is difficult to determine the exact value since it varies in different specimens due to the parameters during growing of CNTs [46]. Moderately thick coating regions up to 2- 3μm at specific reaction time and temperature are also reported [77,78]. Moreover, Deng et al. [79] demonstrated that the quality and quantity of depositing

nanomaterials on the carbon fiber were increased and improved by introducing the ultrasonic during the electrophoresis deposition (EPD) process.

Our models which their results are represented in Fig.9 encompass CCR thicknesses of 500 nm, 700 nm, 900 nm and 1.1 μm with the same CNT volume fraction in order to scrutinize the effect of mere coating thickness on the residual stresses.

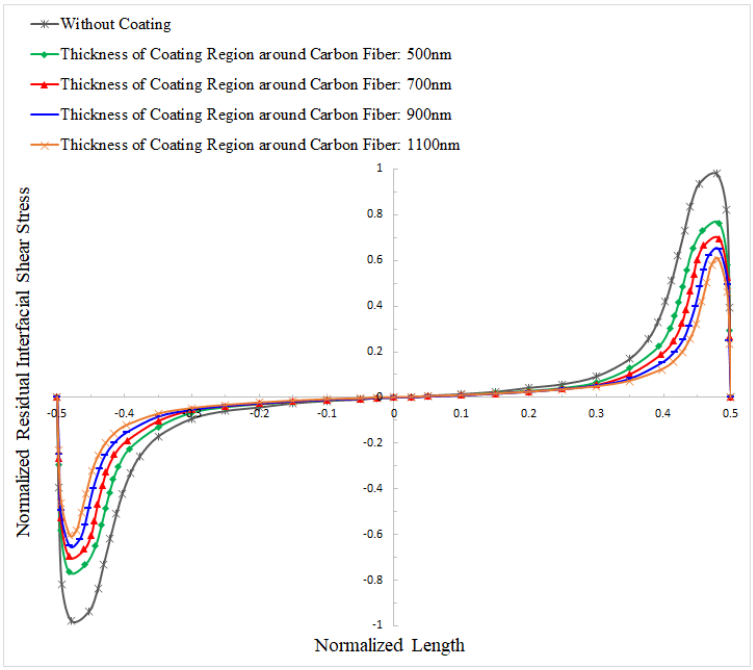

(a)

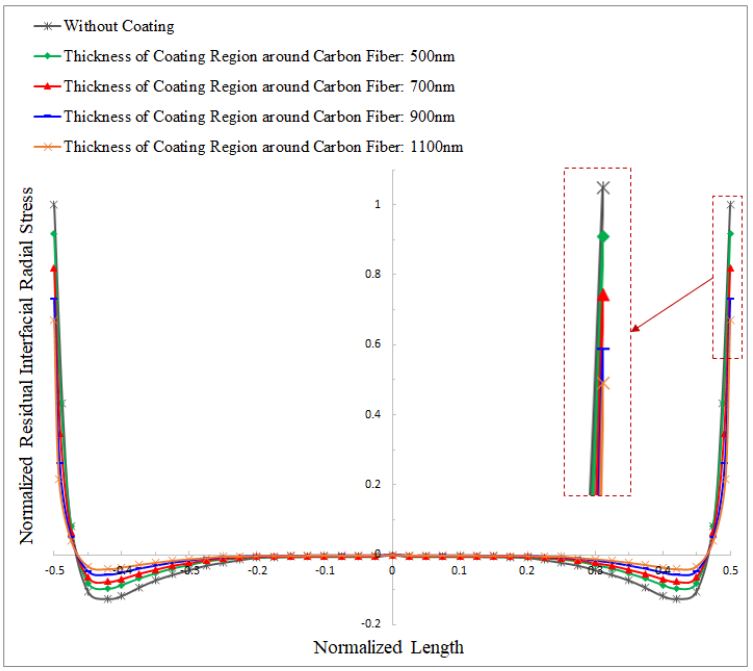

(b)

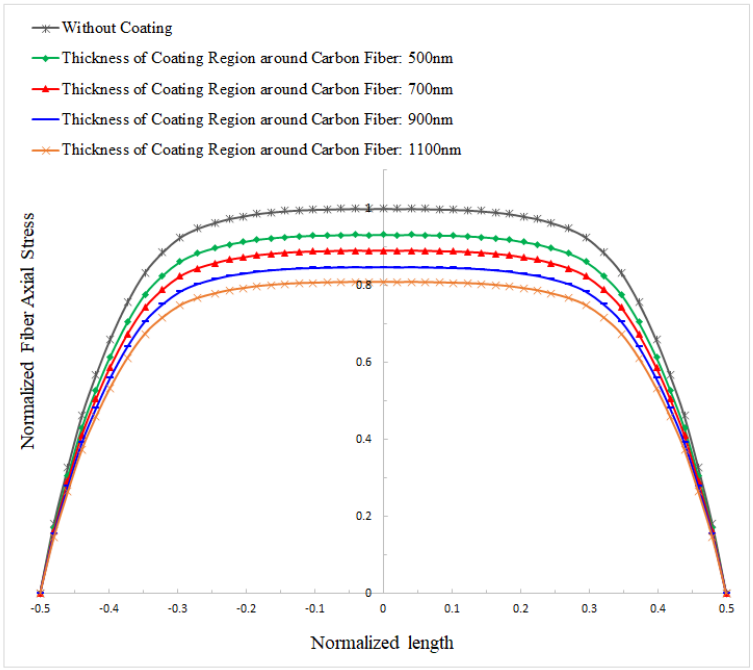

(c)

Fig. 9: Distribution of thermal residual interfacial stresses of hybrid composite at different coating thickness (a) Shear stress (b) Radial stress (c) Fiber axial stress

Our results indicate that increasing the coating thickness around carbon fiber leads towards the reduction of residual interfacial shear (Fig. 9a) and radial (Fig. 9b) stresses as well as the fiber axial stress (Fig. 9c). Even the lowest coating thickness (green curves) decrease the residual stresses remarkably in comparison with the case without coating (gray curves). However, it is observed that the rate of such diminishing effect on residual stresses reduces slightly as the coating thickness enlarges. Moreover, it is manifested from Fig. 9c that the maximum axial stress of fiber occurs at the mid-span, remains almost constant over 80% of the fiber length (slight differences for various coating thicknesses), and plummets near the end of the carbon fiber. Notwithstanding the small portion of CNT at the coating region with a thickness of 1.1μm, the residual interfacial shear and radial stresses and fiber axial stress drop by 39.6 %, 32.8 % and 19.6 %, respectively.

Fig.10 describes the influence of temperature variations magnitude (ΔT) on the residual interfacial stresses and axial fiber stress for a hybrid composite with 1μm thickness of RNCCR. The results indicate that the distributions of stresses for different ΔTs are analogous, and their magnitude increases with elevating ΔT. The minimizing effect of coating on the thermal residual stresses, however, is more effective for higher magnitudes of ΔT. According to Fig. 10a, RNCCR reduces the maximum residual shear stress by 29.1 % and 37.6 % for ΔT= 50 K and ΔT= 100 K, respectively. Likewise, utilizing fiber coating leads to decrease of fiber axial stress by 14.2 % and 18.1 % for ΔT= 50 K and ΔT= 100 K, respectively (see Fig. 10c), which indicates that the coating medium around core fiber makes a notable contribution towards decreasing the interfacial stresses and therefore load transferring phenomenon between fiber and matrix.

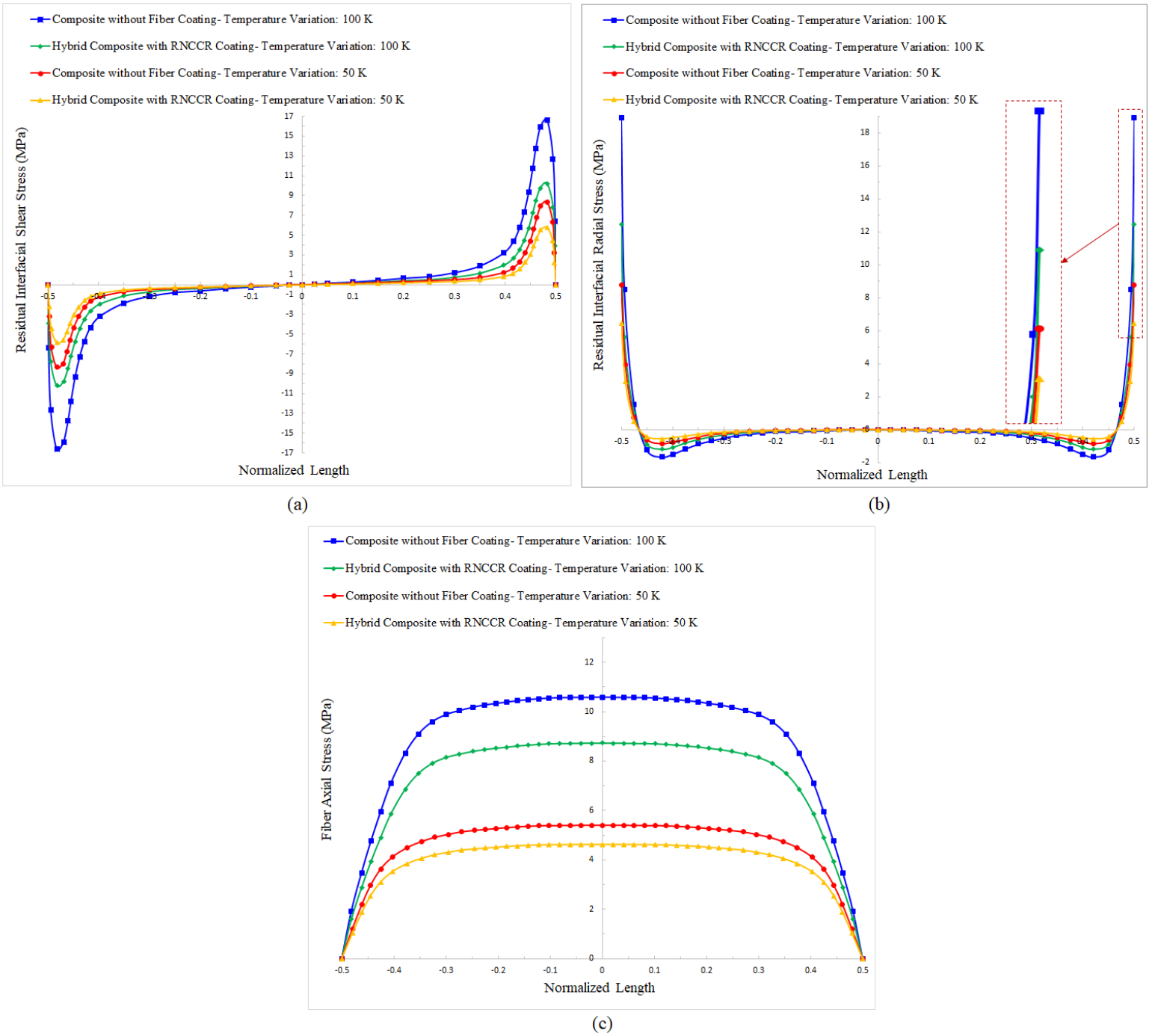

Fig. 10: Distribution of thermal residual interfacial stresses of hybrid composite at different temperature variations (a) Shear stress (b) Radial stress (c) Fiber axial stress with coating thickness of 1 μm

Fig.11 illustrates simultaneously the influence of various coating types (RCCR, RNCCR and ACCR) with different thicknesses on maximum interfacial shear and radial stresses and fiber axial stress, for 1% volume fraction (V_f) of CNTs at each coating region and ΔT= 100 K. The maximum

stresses are normalized by the maximum stresses of composite without fiber coating. A glance at the figures provided shows the extraordinary influence of coating with ACCR and RNCCR in which by increasing the coating thickness, the maximum interfacial stresses fall gradually. In contrast, RCCR exhibits low contribution to the reduction of maximum interfacial stresses and fiber axial stress, even for high coating thicknesses.

According to Fig. 11, a considerable reduction of 23.8%, 30%, 35.1% and 39.5% is gained in maximum residual interfacial shear stress of hybrid composites with RNCCR thicknesses of 0.5μm, 0.7μm, 0.9μm and 1.1μm, respectively. Similarly, their interfacial radial stress falls remarkably in comparison with composites without coatings, although the reducing rate is slightly lower than residual interfacial shear stress. The fiber axial stress, however, is the lowest influenced stress in the case of RNCCR, with decrease percentages of 6.8%, 11%, 15.3% and 20.1% for the aforementioned coating thicknesses.

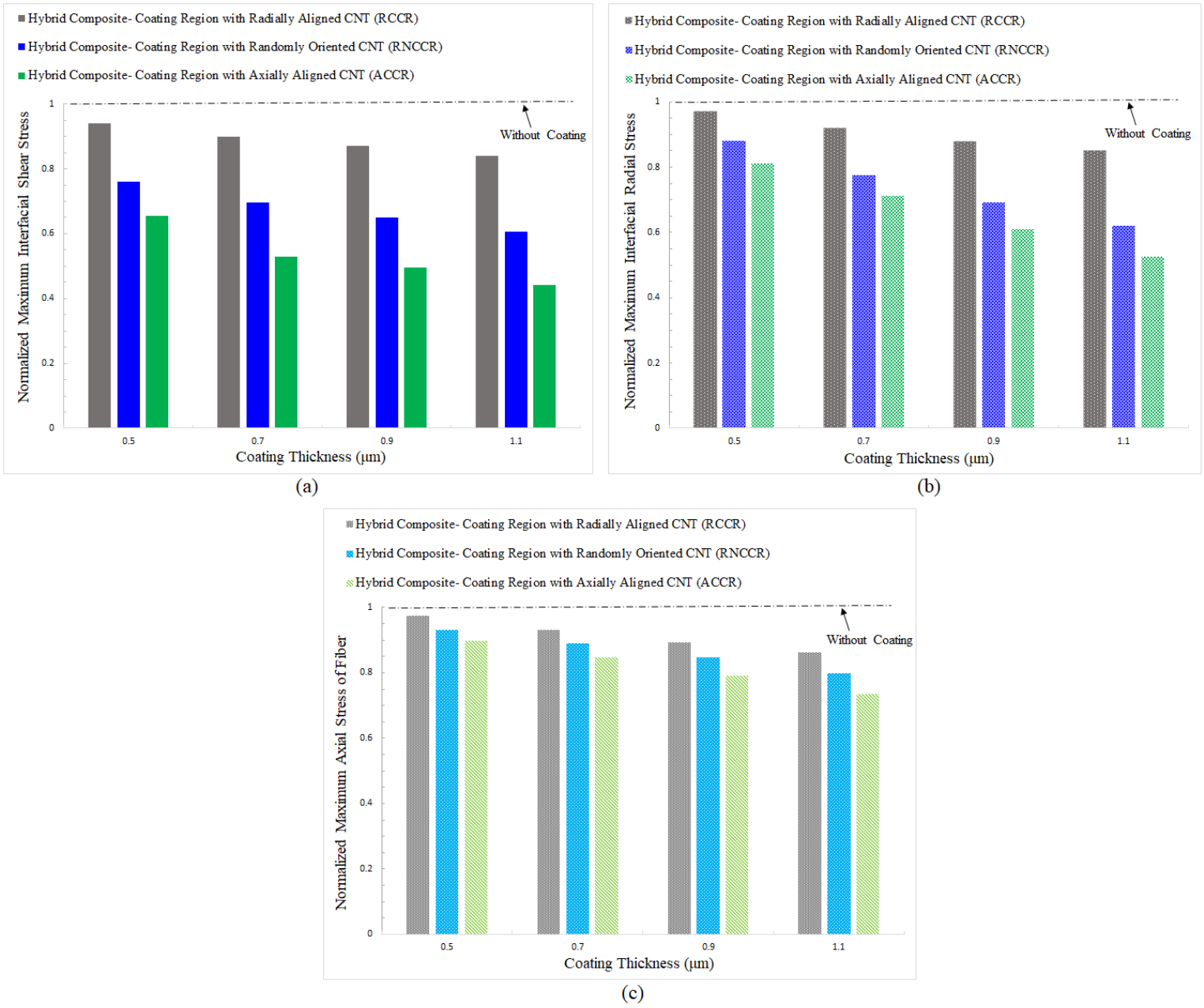

Fig. 11: Normalized maximum stresses versus different coating thicknesses and CNT's orientations (a) Interfacial shear stress (b) Interfacial radial stress (c) Fiber axial stress

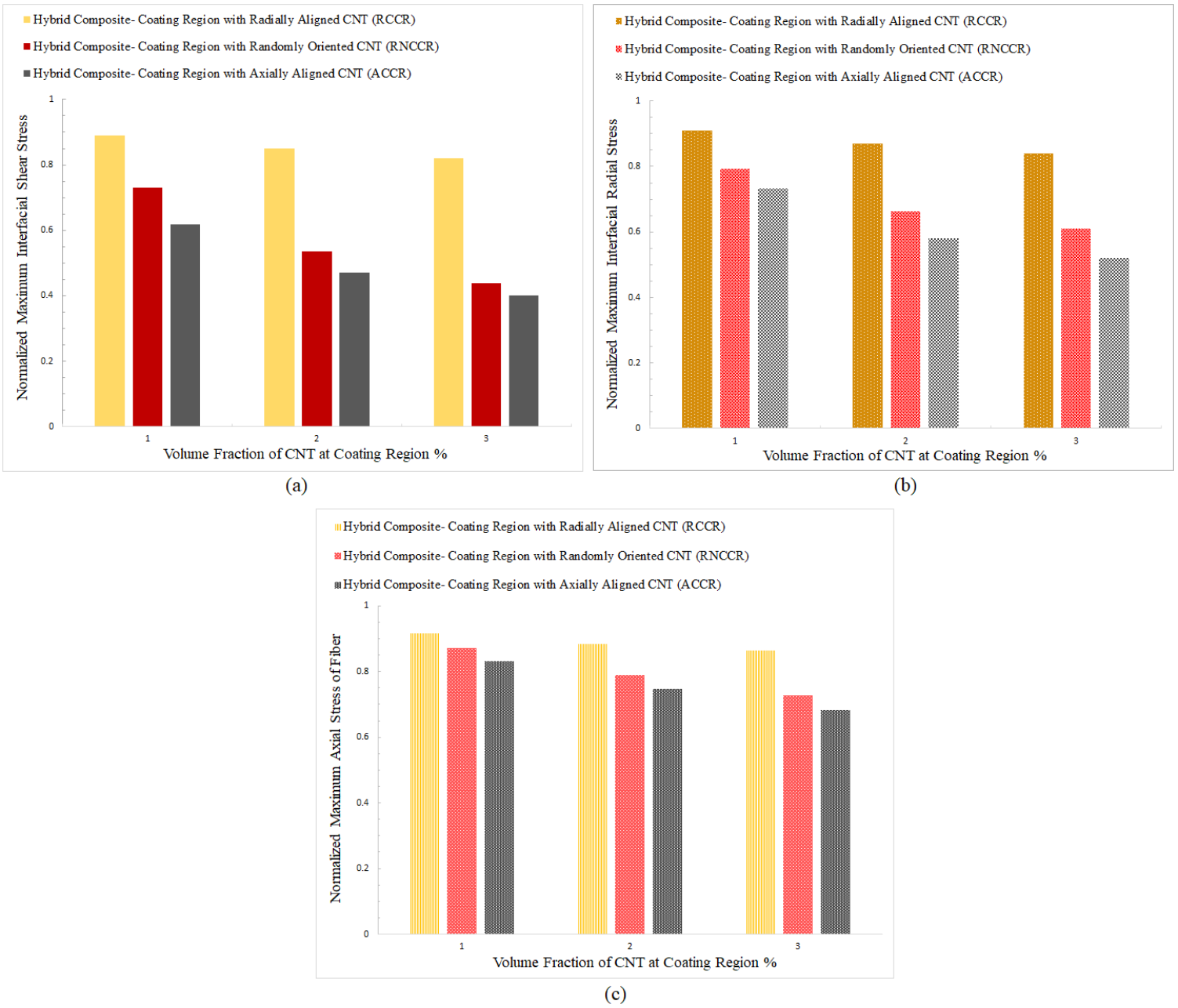

Fig. 12: Normalized maximum stresses versus different CNT volume fractions and CNT's orientations (a) Interfacial Shear stress (b) Interfacial radial stress (c) Fiber axial stress

Fig.12 portrays simultaneously the effect of the coating types and CNT volume fractions on the maximum interfacial shear and radial stresses and maximum fiber axial stress, for a coating thickness of 900 nm and ΔT= 50 K. The hybrid composite models containing RNCCR and ACCR demonstrate noteworthy improvement on the interfacial properties (Fig. 12a-b) and fiber axial stress (Fig. 12c) while RCCR makes a trivial contribution especially at lower CNT volume

fractions. Among the attained stresses, the utmost improvement is acquired in hybrid composite with RNCCR in which the residual interfacial shear stress reduces by 27.2%, 47.3% and 55.4% for CNT volume fractions of 1%, 2% and 3%, respectively. Moreover, taking into account 1%, 2% and 3% of CNT volume fractions yields considerable decrease of fiber axial stress as 13%, 21% and 27.2%, respectively.

5. Conclusion

The present work is allocated to scrutinize the influence of carbon nanotube-coated carbon fibers on the thermal residual stresses of multi-scale hybrid composites. The established model includes unidirectional carbon fiber, coating region and surrounding matrix, in which the coating region around core fiber encompasses CNT and the polymer matrix. Three types of coating regions are considered around carbon fiber based on the three different configurations of grown CNTs on the fiber surface comprising axially, radially and randomly oriented CNTs. Employing the Eshelby–Mori–Tanaka method in conjunction with an equivalent continuum approach, the mechanical properties of three different coating regions are acquired. Consequently, the closed-form solution of the thermal residual stresses of multi- scale hybrid composite is attained utilizing the total complementary energy minimization method. The results reveal an extraordinary decrease in the residual interfacial shear and radial stresses by 27% and 21%, respectively, in the hybrid composite with a coating region consisting of solely 1wt. % of randomly oriented CNTs. Significantly, the mentioned reduction of the interfacial residual stresses not only precludes the deboning between the fiber and matrix, but also attenuates the effect of coefficient of thermal expansions mismatch between the carbon fiber and surrounding matrix. Furthermore, the results manifest a noticeable reduction of interfacial shear stress in the models with coating region comprising axially (ACCR) and randomly oriented CNTs (RNCCR) by 36.5% and 27%, respectively, whereas coating region with radially oriented CNTs make a slight contribution. Likewise, it is disclosed that increasing the coating thickness reduces the maximum interfacial shear stress, radial stress and fiber axial stress by 39.6 %, 32.8 % and 19.6 %, respectively, considering coating thickness of 1.1μm and small portion of CNTs at coating region.

Appendix A

The **A** tensor parameters are given as below [60]:

$$a_1 = (-1+2\upsilon_m)\,[E_m + 2k_{ENF}(1+\upsilon_m)]$$
$$a_2 = E_m + 2m_{ENF}(3-\upsilon_m - 4\upsilon_m{}^2)$$
$$a_3 = E_m(1-\upsilon_m)\left\{E_m(3-4\upsilon_m) + 2(1+\upsilon_m)\,[m_{ENF}(3-4\upsilon_m) + k_{ENF}(2-4\upsilon_m)]\right\}$$
$$a_4 = E_m(1-\upsilon_m)\left\{E_m(1-4\upsilon_m) + 2(1+\upsilon_m)\,[m_{ENF}(3-4\upsilon_m) + k_{ENF}(2-4\upsilon_m)]\right\}$$

Appendix B

The Hill's constants of reinforcement phase are obtained using below equations [57]:

$$\alpha_{ENF} = \frac{3(K_m+G_m)+k_{ENF}-l_{ENF}}{3(G_m+k_{ENF})}$$

$$\beta_{ENF} = \frac{1}{5}\left\{\frac{4G_m+2k_{ENF}+l_{ENF}}{3(G_m+k_{ENF})} + \frac{4G_m}{G_m+p_{ENF}} + \frac{2\,[G_m(3K_m+G_m)+G_m(3K_m+7G_m)]}{G_m(3K_m+G_m)+m_{ENF}(3K_m+7G_m)}\right\}$$

$$\delta_{ENF} = \frac{1}{3}\left[n_{ENF}+2l_{ENF} + \frac{(2k_{ENF}+l_{ENF})(3K_m+2G_m-l_{ENF})}{G_m+k_{ENF}}\right]$$

$$\eta_{RNF} = \frac{1}{5}\left[\frac{2}{3}(n_{ENF}-l_{ENF}) + \frac{8G_m\,p_{ENF}}{G_m+p_{ENF}} + \frac{8\,m_{ENF}\,G_m(3K_m+4G_m)}{3K_m(m_{ENF}+G_m)+G_m(7m_{ENF}+G_m)} + \frac{2\,(k_{ENF}-l_{ENF})(2G_m+l_{ENF})}{3(G_m+k_{ENF})}\right]$$

Appendix C

Regarding CNT-coating interphase (CCR), the integrations of normal, shear and radial stresses at this region are calculated as following. Thus, considering the term regarding axial stress in CCR:

$$\frac{1}{2}\sigma^{zz}_{ACCR}\varepsilon^{zz}_{ACCR} = \frac{1}{2}\sigma^{zz}_{ACCR}\,[\frac{1}{E^z_{ACCR}}(\sigma^{zz}_{ACCR} - 2\upsilon^z_{ACCR}\sigma^{rr}_{ACCR}) + \alpha^z_{ACCR}\Delta T]$$
$$= \frac{1}{2E^z_{ACCR}}(\sigma^{zz}_{ACCR})^2 - \frac{\upsilon^z_{ACCR}}{E^z_{ACCR}}\sigma^{zz}_{ACCR}\sigma^{rr}_{ACCR} + \frac{1}{2}\sigma^{zz}_{ACCR}\alpha^z_{ACCR}\Delta T \qquad \text{(C.1)}$$

Hence, by substituting the stresses in terms of $g_1(z)$ and $g_2(z)$ obtained by Eq (33) & (41) into (C.1), the integral related to axial stress is expressed as:

$$\iiint_v \left(\frac{1}{2}\sigma^{zz}_{ACCR}\varepsilon^{zz}_{ACCR}\right) r\,dr\,d\theta\,dz \tag{C.2}$$

$$= \iiint_v \left[\frac{B_2^2}{2E^z_{ACCR}} g_2(z)^2 - \frac{\upsilon^z_{ACCR}}{E^z_{ACCR}} B_2\, g_2(z) \left\{ -\frac{B_1}{4}\frac{d^2 g_1(z)}{dz^2}\left(2R_f^2 \ln R_m - (R_m^2 - 2R_{CCR}^2 \ln R_m)\frac{V_f}{V_m} + (R_{CCR}^2 - 2R_{CCR}^2 \ln R_{CCR})\frac{V_f}{V_m} - 2R_f^2 \ln r \right) - \frac{B_2}{4}\frac{d^2 g_2(z)}{dz^2}\left(2(R_{CCR}^2 - R_f^2)\ln R_m - (R_m^2 - 2R_{CCR}^2 \ln R_m)\frac{V_{CCR}}{V_m} - 2(R_{CCR}^2 - R_f^2)\ln R_{CCR} + (R_{CCR}^2 - 2R_{CCR}^2 \ln R_{CCR})\frac{V_{CCR}}{V_m} - 2R_f^2 \ln R_{CCR} + R_{CCR}^2 + 2R_f^2 \ln r - r^2 \right) \right\} + \frac{1}{2} B_2 g_2(z) \alpha^z_{ACCR} \Delta T \right] r\,dr\,d\theta\,dz$$

The integration with respect to r from R_f to R_{CCR} is performed as below:

$$\int_{R_f}^{R_{CCR}} \left(\frac{1}{2}\sigma^{zz}_{ACCR}\varepsilon^{zz}_{ACCR}\right) r\,dr \tag{C.3}$$

$$= \frac{1}{4E_{ccrz}(-1+V_f)}\left(\left(-\left(-(R_f + R_{ccr})(R_f - R_{ccr})((V_{ccr} - V_f + 1)R_{ccr}^2 + R_f^2(-1+V_f))ln(R_m) - 2R_{ccr}^2\left(\left(-\frac{V_f}{2} + \frac{V_{ccr}}{2} + \frac{1}{2}\right)R_{ccr}^2 + R_f^2\left(V_f - \frac{V_{ccr}}{2} - 1\right)\right)ln(R_{ccr}) + R_f^4(-1+V_f)ln(R_f) - \frac{3}{4}(R_f + R_{ccr})(R_f - R_{ccr})\left(\left(-\frac{V_f}{3} + \left(\frac{2V_{ccr}}{3} + \frac{1}{3}\right)R_{ccr}^2 + R_f^2(-1+V_f) - \left(\frac{2}{3}R_m^2 V_\partial\right)\right)\upsilon_{ccrz} B_2 \left(\frac{d^2}{dz^2} g_2(z)\right) + \left(-(R_f + R_{ccr})(R_f - R_{ccr})(-R_{ccr}^2 V_f + R_f^2(-1+V_f))ln(R_m) + (R_{ccr}^4 Vf - 2Rf^2(V_f - \frac{1}{2})R_{ccr}^2)ln(R_{ccr}) + R_f^4(-1+V_f)ln(R_f) - \frac{1}{2}(-R_{ccr}^2 V_f + R_f^2(-1+V_f) + R_m^2 V_f (R_f + R_{ccr})(R_f - R_{ccr}))\upsilon_{ccrz} B_1 \left(\frac{d^2}{dz^2} g_1(z)\right) - (R_f - R_{ccr})(R_f + R_{ccr})(-1 + V_f)(\alpha_{ccrz}\Delta T E_{ccrz} + B_2 g_2(z))\right) B_2 g_2(z)\right)$$

From Eq (54), the term related to shear stress in Eq (56) is stated as:

$$\tau^{rz}_{ACCR}\varepsilon^{rz}_{ACCR} = \frac{1}{2G_{ACCR}}(\tau^{rz}_{ACCR})^2 \quad , \quad G^z_{ACCR} = \frac{E^z_{ACCR}}{2(1+\upsilon^Z_{ACCR})}$$

Then: (C.4)

$$\tau^{rz}_{ACCR}\varepsilon^{rz}_{ACCR} = \frac{1+\upsilon^Z_{ACCR}}{E^z_{ACCR}}(\tau^{rz}_{ACCR})^2$$

Thus, by substituting the CCR's shear stress in terms of $g_1(z)$ and $g_2(z)$ obtained by Eq (40) into (C.4):

$$\iiint_v (\tau^{rz}_{ACCR}\varepsilon^{rz}_{ACCR})\, r\, dr\, d\theta\, dz = \iiint_v \left[\frac{1+\upsilon^{Z}_{ACCR}}{E^{z}_{ACCR}}(\tau^{rz}_{ACCR})^2\right] r\, dr\, d\theta\, dz$$

$$= \iiint_v \left[\frac{1+\upsilon^{Z}_{ACCR}}{E^{z}_{ACCR}}\left(\frac{1}{4r^2}\left\{B_1 {R_f}^2 \frac{\mathrm{d}g_1(z)}{\mathrm{d}z} + B_2(r^2 - {R_f}^2)\frac{\mathrm{d}g_2(z)}{\mathrm{d}z}\right\}^2\right)\right] r\, dr\, d\theta\, dz \qquad \text{(C.5)}$$

The integration with respect to r from R_{CCR} to R_m is accomplished accordingly:

$$\int_{R_f}^{R_{CCR}} (\tau^{rz}_{ACCR}\varepsilon^{rz}_{ACCR})\, r\, dr$$

$$= -\frac{1+\upsilon_{ccrz}}{4E_{ccrz}}\left(\left(ln(R_f){R_f}^4 - ln(R_{ccr}){R_f}^4 - \frac{3{R_f}^4}{4} + {R_{ccr}}^2{R_f}^2 - \frac{{R_{ccr}}^4}{4}\right){B_2}^2\left(\frac{d}{dz}g_2(z)\right)^2 - 2{R_f}^2 B_1\left({R_f}^2\right.\right. \qquad \text{(C.6)}$$

$$\left.\left. ln(R_f) - {R_f}^2 ln(R_{ccr}) - \frac{{R_f}^2}{2} + \frac{{R_{ccr}}^2}{2}\right)B_2\left(\frac{d}{dz}g_1(z)\right)\left(\frac{d}{dz}g_2(z)\right) + {B_1}^2\left(\frac{d}{dz}g_1(z)\right)^2 {R_f}^4 (ln(R_f) - ln(R_{ccr}))\right)$$

With the same procedure for shear and axial stresses, the radial stress of CCR is acquired as following:

$$\frac{1}{2}\sigma^{rr}_{ACCR}\varepsilon^{rr}_{ACCR} = \frac{1}{2}\sigma^{rr}_{ACCR}\left[\frac{1}{E^{r}_{ACCR}}(\sigma^{rr}_{ACCR} - \upsilon^{r}_{ACCR}(\sigma^{zz}_{ACCR} - \sigma^{\theta\theta}_{ACCR}) + \alpha^{r}_{ACCR}\Delta T\right] \qquad \text{(C.7)}$$

$$= \frac{1}{2E^{r}_{ACCR}}(\sigma^{rr}_{ACCR})^2 - \frac{\upsilon^{r}_{ACCR}}{2E^{r}_{ACCR}}\sigma^{rr}_{ACCR}\sigma^{zz}_{ACCR} - \frac{\upsilon^{r}_{ACCR}}{2E^{r}_{ACCR}}\sigma^{rr}_{ACCR}\sigma^{\theta\theta}_{ACCR} + \frac{1}{2}\sigma^{rr}_{ACCR}\alpha^{r}_{ACCR}\Delta T$$

$$\int_{R_f}^{R_{CCR}} \left(\frac{1}{2}\sigma_{ACCR}^{rr}\varepsilon_{ACCR}^{rr}\right) r\,dr \qquad \text{(C.8)}$$

$$= \frac{1}{384\,E_{ccrr}\,(V_f-1)^2}(24(\upsilon_{ccrr}-)((R_f+R_{ccr})(R_f-R\,ccr)((V_{ccr}-V_f+1)R_{ccr}^{\ 2}+R_f^{\ 2}(-1+V_f))^2 ln(R_m)^2-2(-2R_{Rccr}^{\ 2}((-\frac{V_f}{2}+\frac{V_{ccr}}{2}+\frac{1}{2})R_{ccr}^{\ 2}$$

$$+R_f^{\ 2}(V_f-\frac{V_{ccr}}{2}-1))ln(R_{ccr})+R_f^{\ 4}(-1+V_f)ln(R_f)-\frac{3}{4}(R_f+R_{ccr})(R_f-R_{ccr})((-\frac{V_f}{3}+\frac{2V_{ccr}}{3}+\frac{1}{3})R_{ccr}^{\ 2}+R_f^{\ 2}(-1+V_f)-(\frac{2R_m^{\ 2}V_{ccr}}{3}))((V_{ccr}$$

$$-V_f+1)R_{ccr}^{\ 2}+R_f^{\ 2}(-1+V_f))ln(R_m)-((V_{ccr}-V_f+1)R_{ccr}^{\ 2}-R_f(V_f-V_{ccr}-1)R_{ccr}-R_f^{\ 2}(-1+V_f))R_{ccr}^{\ 2}((V_{ccr}-V_f+1)R_{ccr}^{\ 2}-R_f(V_f-V_{ccr}$$

$$-1)R_{ccr}+R_f^{\ 2}(-1+V_f))ln(R_{ccr})^2-2R_{ccr}^{\ 2}(R_f^{\ 4}(-1+V_f)(V_f-V_{ccr}-1)ln(R_f)-\frac{1}{4}(V_f-V_{ccr}-1)(V_f-2V_{ccr}-1)R_{ccr}^{\ 4}+((\frac{5}{4}V_f^{\ 2}+(\frac{-5}{2}-$$

$$2V_{ccr})V_f+2V_{ccr}+\frac{5}{4}+\frac{V_{ccr}^{\ 2}}{2})R_f^{\ 2}-\frac{1}{2}R_m^{\ 2}V_{ccr}(V_f-V_{ccr}-1))R_{ccr}^{\ 2}-\frac{5}{4}R_f^{\ 2}((-1+V_f)(V_f-\frac{3V_{ccr}}{5}-1)R_f^{\ 2}-\frac{4}{5}(V_f-\frac{V_{ccr}}{2}-1)V_{ccr}R_m^{\ 2}))ln(R_{ccr})$$

$$+R_f^{\ 6}(-1+V_f)^2 ln(R_f)^2-\frac{3}{2}R_f^{\ 4}((-\frac{2}{3}V_f+\frac{2}{3}V_{ccr}+\frac{2}{3})R_{ccr}^{\ 2}+R_f^{\ 2}(-1+V_f)-\frac{2R_m^{\ 2}V_{ccr}}{3})(-1+V_f)ln(R_f)\frac{1}{24}((2V_f^{\ 2}+(-6V_{ccr}-4)V_f+6V_{ccr}^{\ 2}$$

$$+6V_{ccr}+2)R_{ccr}^{\ 4}+(-13(-1+V_f)(V_f-(\frac{18V_{ccr}}{13}-1)R_f^{\ 2}+6R_m^{\ 2}V_{ccr}(V_f-2V_{ccr}-1))R_{ccr}^{\ 2}+17(-1+V_f)^2R_f^{\ 4}-18R_m^{\ 2}V_{ccr}(-1+V_f)R_f^{\ 2}+(6R_m^{\ 4}$$

$$V_{ccr}^{\ 2})(R_f+R_{ccr})(R_f-R_{ccr}))\,B_2^{\ 2}\left(\frac{d^2}{dz^2}g_1(z)\right)^2-48(\upsilon_{ccrr}-1)((R_f+R_{ccr})(R_f-R_{ccr})((V_{ccr}-V_f+1)R_{ccr}^{\ 2}+R_f^{\ 2}(-1+V_f))(-R_{ccr}^{\ 2}V_f+R_f^{\ 2}(-1$$

$$+V_f))ln(R_m)^2+(4R_{ccr}^{\ 2}(\frac{1}{2}V_f(V_f-V_{ccr}-1)R_{ccr}^{\ 4}-\frac{3}{2}R_f^{\ 2}(V_f^{\ 2}+(-\frac{2V_{ccr}}{3}-\frac{4}{3})V_f+\frac{V_{ccr}}{3}+\frac{1}{3})R_{ccr}^{\ 2})+R_f^{\ 4}(-1+V_f)(V_f-\frac{V_{ccr}}{4}-\frac{3}{4}))ln(R_{ccr})$$

$$-2R_f^{\ 4}(-1+V_f)((-V_f+\frac{V_{ccr}}{2}+\frac{1}{2})R_{ccr}^{\ 2}+R_f^{\ 2}(-1+V_f))ln(R_f)+(\frac{5}{4}(\frac{3}{5}V_f(V_f-\frac{4V_{ccr}}{3}-1)R_{ccr}^{\ 4})+(-\frac{8}{5}(-1+V_f)(V_f-\frac{V_{ccr}}{2}-\frac{3}{8})R_f^{\ 2})-(\frac{2}{5}$$

$$R_m^{\ 2}V_f(V_f-2V_{ccr}-1))R_{ccr}^{\ 2}+R_f^{\ 2}(R_f^{\ 2}(-1+V_f)+\frac{2R_m^{\ 2}(V_f-V_{ccr})}{5})(-1+V_f))(R_f+R_{ccr})(R_f-R_{ccr}))\ln(R_m)-R_{ccr}^{\ 2}(V_f(V_f-V_{ccr}-1)R_{ccr}^{\ 4}$$

$$-3R_f^{\ 2}(V_f^{\ 2}+(-\frac{2}{3}V_{ccr}-\frac{4}{3})V_f+\frac{V_{ccr}}{3}+\frac{1}{3})R_{ccr}^{\ 2}+(-1+V_f)^2R_f^{\ 4})ln(R_{ccr})^2-2R_{ccr}^{\ 2}(R_f^{\ 4}(-1+V_f)(V_f-\frac{V_{ccr}}{2}-\frac{1}{2})ln(R_f)-\frac{3}{8}V_f(V_f-\frac{4V_{ccr}}{3}$$

$$-1)R_{ccr}^{\ 4})+((\frac{11}{8}V_f^{\ 2}+(-\frac{7}{4}-V_{ccr})V_f+\frac{V_{ccr}}{2}+\frac{3}{8})R_f^{\ 2}+\frac{1}{4}R_m^{\ 2}V_f(V_f-2V_{ccr}-1))R_{ccr}^{\ 2}-\frac{9}{8}R_f^{\ 2}((V_f-\frac{2V_{ccr}}{9}-\frac{2}{3})(-1+V_f)R_f^{\ 2}+\frac{4}{9}R_m^{\ 2}(V_f^{\ 2}+$$

$$(-\frac{3V_{ccr}}{2}-1)V_f+\frac{V_{ccr}}{2})))ln(R_{ccr})+R_f^{\ 6}(-1+V_f)^2ln(R_f)^2-\frac{5}{4}R_f^{\ 4}(-1+V_f)((-\frac{4}{5}V_f+\frac{2V_{ccr}}{5}+\frac{2}{5})R_{ccr}^{\ 2}+R_f^{\ 2}(-1+V_f)+\frac{2}{5}R_m^{\ 2}(V_f-V_{ccr}))$$

$$ln(R_f)+\frac{9}{16}(\frac{2V_f}{9}(V_f-2V_{ccr}-1)R_{ccr}^{\ 4})+(-(-1+V_f)(V_f-\frac{4V_{ccr}}{9}-\frac{1}{3})R_f^{\ 2}-(\frac{2}{9}R_m^{\ 2}V_f(V_f-4V_{ccr}-1))R_{ccr}^{\ 2}+(-1+V_f)^2R_f^{\ 4}+\frac{2}{3}(-1+V_f)$$

$$R_m^{\ 2}(V_f-\frac{2}{3}V_{ccr})R_f^{\ 2}-\frac{4R_m^{\ 4}V_fV_{ccr}}{9})(R_f+R_{ccr})(R_f-R_{ccr})B_1\left(\frac{d^2}{dz^2}g_1(z)\right)-(-(R_f+R_{ccr})(R_f-R_{ccr})((V_{ccr}-V_f+1)R_{ccr}^{\ 2}+R_f^{\ 2}(-1+V_f))$$

$$ln(R_m)-2R_{ccr}^{\ 2}((-\frac{Vf}{2}+\frac{V_{ccr}}{2}+\frac{1}{2})R_{ccr}^{\ 2}+R_f^{\ 2}(V_f-\frac{V_{ccr}}{2}-1))ln(R_{ccr})+R_f^{\ 4}(-1+V_f)ln(R_f)-\frac{3}{4}(R_f+R_{ccr})(R_f-R_{ccr})((-\frac{V_f}{3}+\frac{2V_{ccr}}{3}+\frac{1}{3})$$

$$R_{ccr}^{\ 2}+R_f^{\ 2}(-1+V_f)-(\frac{2R_m^{\ 2}V_{ccr}}{3}))(-1\ +\ V_f)(E_{ccrr}\alpha_{ccrr}\Delta T-\upsilon_{ccrr}B_2g_2(z)))B_2\left(\frac{d^2}{dz^2}g_2(z)\right)+24\left(\frac{d^2}{dz^2}g_1(z)\right)(\upsilon_{ccrr}\ -\ 1)((R_f+R_{ccr})(R_f-$$

$$R_\partial)(-R_{ccr}^{\ 2}V_f+R_f^{\ 2}(-1+Vf))^2ln(R_m)^2-2((R_{ccr}^{\ 4}V_f-2R_f^{\ 2}(V_f-\frac{1}{2})R_{ccr}^{\ 2})ln(R_{ccr})+R_f^{\ 4}(-1+V_f)ln(R_f)-\frac{1}{2}(-R_{ccr}^{\ 2}V_f+R_f^{\ 2}(-1+V_f)+$$

$$R_m^{\ 2}V_f)(R_f+R_{ccr})(R_f-R_{ccr}))(-R_{ccr}^{\ 2}V_f+R_f^{\ 2}(-1+V_f))ln(R_m)+\frac{1}{2}(\frac{R_{ccr}^{\ 4}V_f^{\ 2}}{2}+((-V_f^{\ 2}+V_f)R_f^{\ 2}-R_m^{\ 2}V_f^{\ 2})R_{ccr}^{\ 2}+(-1+V_f)^2R_f^{\ 4}+R_m^{\ 2}V_f$$

$$(-1+V_f)R_f^{\ 2}+\frac{R_m^{\ 4}V_f^{\ 2}}{2})(R_f+R_{ccr})(R_f-R_{ccr}))B_1\left(\frac{d^2}{dz^2}g_1(z)\right)-2(-(R_f+R_{ccr})(R_f-R_{ccr})(-R_{ccr}^{\ 2}V_f+R_f^{\ 2}(-1+V_\partial))ln(R_m)+(R_{ccr}^{\ 4}V_f$$

$$-2R_f^{\ 2}(V_f-\frac{1}{2})R_{ccr}^{\ 2})ln(R_{ccr})+R_f^{\ 4}(-1+V_f)\ln(R_f)-\frac{1}{2}(-R_{ccr}^{\ 2}V_f+R_f^{\ 2}(-1+V_f)+R_m^{\ 2}V_f)(R_f+R_{ccr})(R_f-R_{ccr}))(-1\ +\ V_f)(E_{ccrr}\alpha_{ccrr}$$

$$\Delta T-\upsilon_{ccrr}B_2g_2(z)))B_1)$$

References

[1] Balaji Thattaiparthasarathy K, Pillay S, Ning H, Vaidya UK. Process simulation, design and manufacturing of a long fiber thermoplastic composite for mass transit application. Compos Part A Appl Sci Manuf 2008;39:1512–21. doi:10.1016/J.COMPOSITESA.2008.05.017.

[2] Chen Z, Tang H, Shao Y, Sun Q, Zhou G, Li Y, et al. Failure of chopped carbon fiber Sheet Molding Compound (SMC) composites under uniaxial tensile loading: Computational prediction and experimental analysis. Compos Part A Appl Sci Manuf 2019;118:117–30. doi:10.1016/J.COMPOSITESA.2018.12.021.

[3] Mouton S, Teissandier D, Sébastian P, Nadeau JP. Manufacturing requirements in design: The RTM process in aeronautics. Compos Part A Appl Sci Manuf 2010;41:125–30. doi:10.1016/J.COMPOSITESA.2009.09.027.

[4] Icardi U, Sciuva M Di, Librescu L. Dynamic response of adaptive cross-ply cantilevers featuring interlaminar bonding imperfections. AIAA J 2000;38:499–506.

[5] Malekimoghadam R, Icardi U. Prediction of mechanical properties of carbon nanotube–carbon fiber reinforced hybrid composites using multi-scale finite element modelling. Compos Part B Eng 2019;177:107405. doi:10.1016/j.compositesb.2019.107405.

[6] Icardi U. Free vibration of composite beams featuring interlaminar bonding imperfections and exposed to thermomechanical loading. Compos Struct 1999;46:229–43. https://doi.org/https://doi.org/10.1016/S0263-8223(99)00058-6.

[7] Icardi U, Urraci A. Considerations about the choice of layerwise and through-thickness global functions of 3-D physically-based zig-zag theories. Compos Struct 2020;244:112233. https://doi.org/https://doi.org/10.1016/j.compstruct.2020.112233.

[8] Kim J-K, Mai Y-W. Engineered interfaces in fiber reinforced composites. Elsevier; 1998.

[9] Shueh CH, Becher PF. Thermal expansion coefficient of unidirectional fiber reinforced ceramics. J Am Ceram Soc 1988; 71: C438–C441.

[10] Kurtz RD, Pagano NJ. Analysis of the deformation of a symmetrically-loaded fiber

embedded in a matrix material. Compos Eng 1991. doi:10.1016/0961-9526(91)90022-K.

[11] Jayaraman K, Reifsnider KL. The interphase in unidirectional fiber-reinforced epoxies: Effect on residual thermal stresses. Compos Sci Technol 1993;47:119–29. doi:10.1016/0266-3538(93)90041-E.

[12] Hobbiebrunken T, Fiedler B, Hojo M, Ochiai S, Schulte K. Microscopic yielding of CF/epoxy composites and the effect on the formation of thermal residual stresses. Compos Sci Technol 2005;65:1626–35. doi:10.1016/J.COMPSCITECH.2005.02.003.

[13] Shokrieh MM, Daneshvar A, Akbari S. Reduction of thermal residual stresses of laminated polymer composites by addition of carbon nanotubes. Mater Des 2014;53:209–16.

[14] Shokrieh MM, Safarabadi M. Three-dimensional analysis of micro-residual stresses in fibrous composites based on the energy method: a study including interphase effects. J Compos Mater 2012;46:727–35.

[15] Aghdam MM, Khojeh A. More on the effects of thermal residual and hydrostatic stresses on yielding behavior of unidirectional composites. Compos Struct 2003;62:285–90. doi:10.1016/J.COMPSTRUCT.2003.09.027.

[16] Zhao LG, Warrior NA, Long AC. A thermo-viscoelastic analysis of process-induced residual stress in fibre-reinforced polymer–matrix composites. Mater Sci Eng A 2007;452–453:483–98. doi:10.1016/J.MSEA.2006.10.060.

[17] Naik R. Simplified Micromechanical Equations for Thermal Residual Stress Analysis of Coated Fiber Composites. J Compos Technol Res 1992;14:182–6. doi:10.1520/CTR10096J.

[18] Arnold SM, Arya VK, Melis ME. Elastic/plastic analyses of advanced composites investigating the use of the compliant layer concept in reducing residual stresses resulting from processing 1990.

[19] Rafiee R, Malekimoghadam R. On the modeling of carbon nanotubes: A critical review. Compos Part B Eng 2014. doi:10.1016/j.compositesb.2013.08.037.

[20] Hosseini SA, Saber-Samandari S, Maleki Moghadam R. Multiscale modeling of interface debonding effect on mechanical properties of nanocomposites. Polym Compos 2017;38:789–96.

[21] Zahedi M, Malekimoghadam R, Rafiee R, Icardi U. A study on fracture behavior of semi-elliptical 3D crack in clay-polymer nanocomposites considering interfacial debonding. Eng Fract Mech 2019;209:245–59.

[22] Moghadam RM, Saber-Samandari S, Hosseini SA. On the tensile behavior of clay–epoxy nanocomposite considering interphase debonding damage via mixed-mode cohesive zone material. Compos Part B Eng 2016;89:303–15.

[23] Vu-Bac N, Lahmer T, Zhang Y, Zhuang X, Rabczuk T. Stochastic predictions of interfacial characteristic of polymeric nanocomposites (PNCs). Compos Part B Eng 2014. doi:10.1016/j.compositesb.2013.11.014.

[24] Kwon, Y.-K., Berber, S., & Tománek, D. (2004). Thermal Contraction of Carbon Fullerenes and Nanotubes. Phys. Rev. Lett., 92(1), 15901. https://doi.org/10.1103/PhysRevLett.92.015901

[25] Romanov V, Lomov S V., Verpoest I, Gorbatikh L. Inter-fiber stresses in composites with carbon nanotube grafted and coated fibers. Compos Sci Technol 2015;114:79–86. doi:10.1016/J.COMPSCITECH.2015.04.013.

[26] Mousavi AA, Arash B, Zhuang X, Rabczuk T. A coarse-grained model for the elastic properties of cross linked short carbon nanotube/polymer composites. Compos Part B Eng 2016;95:404–11.

[27] Shen Z, Bateman S, Wu DY, McMahon P, Dell'Olio M, Gotama J. The effects of carbon nanotubes on mechanical and thermal properties of woven glass fibre reinforced polyamide-6 nanocomposites. Compos Sci Technol 2009;69:239–44. doi:10.1016/J.COMPSCITECH.2008.10.017.

[28] Qian D, Dickey EC, Andrews R, Rantell T. Load transfer and deformation mechanisms in carbon nanotube-polystyrene composites. Appl Phys Lett 2000;76:2868–70.

[29] Rodriguez AJ, Guzman ME, Lim C-S, Minaie B. Mechanical properties of carbon

nanofiber/fiber-reinforced hierarchical polymer composites manufactured with multiscale-reinforcement fabrics. Carbon N Y 2011;49:937–48.

[30] Ray MC, Kundalwal SI. A thermomechanical shear lag analysis of short fuzzy fiber reinforced composite containing wavy carbon nanotubes. Eur J Mech - A/Solids 2014;44:41–60. doi:10.1016/J.EUROMECHSOL.2013.10.001.

[31] Kundalwal SI, Meguid SA. Micromechanics modelling of the effective thermoelastic response of nano-tailored composites. Eur J Mech - A/Solids 2015;53:241–53. doi:10.1016/J.EUROMECHSOL.2015.05.008.

[32] Kundalwal SI, Ray MC. Effect of carbon nanotube waviness on the effective thermoelastic properties of a novel continuous fuzzy fiber reinforced composite. Compos Part B Eng 2014;57:199–209. doi:10.1016/J.COMPOSITESB.2013.10.003.

[33] Chatzigeorgiou, G., Meraghni, F., Charalambakis, N., & Benaarbia, A. (2020). Multiscale modeling accounting for inelastic mechanisms of fuzzy fiber composites with straight or wavy carbon nanotubes. International Journal of Solids and Structures, 202, 39–57. https://doi.org/https://doi.org/10.1016/j.ijsolstr.2020.05.015

[34] Chatzigeorgiou, G., Efendiev, Y., & Lagoudas, D. C. (2011). Homogenization of aligned "fuzzy fiber" composites. International Journal of Solids and Structures, 48(19), 2668–2680. https://doi.org/https://doi.org/10.1016/j.ijsolstr.2011.05.011

[35] Chatzigeorgiou, G., Seidel, G. D., & Lagoudas, D. C. (2012). Effective mechanical properties of "fuzzy fiber" composites. Composites Part B: Engineering, 43(6), 2577–2593.

[36] Karami G, Garnich M. Micromechanical study of thermoelastic behavior of composites with periodic fiber waviness. Compos Part B Eng 2005;36:241–8. doi:10.1016/J.COMPOSITESB.2004.09.005.

[37] Quek MY. Analysis of residual stresses in a single fibre–matrix composite. Int J Adhes Adhes 2004;24:379–88. doi:10.1016/S0143-7496(03)00097-6.

[38] Mikata Y, Taya M. Stress Field in a Coated Continuous Fiber Composite Subjected to Thermo-Mechanical Loadings. J Compos Mater 1985;19:554–78.

doi:10.1177/002199838501900607.

[39] Honjo K. Thermal stresses and effective properties calculated for fiber composites using actual cylindrically-anisotropic properties of interfacial carbon coating. Carbon N Y 2007;45:865–72.

[40] Bekyarova E, Thostenson ET, Yu A, Kim H, Gao J, Tang J, et al. Multiscale Carbon Nanotube−Carbon Fiber Reinforcement for Advanced Epoxy Composites. Langmuir 2007;23:3970–4. doi:10.1021/la062743p.

[41] Li Q, Church JS, Naebe M, Fox BL. Interfacial characterization and reinforcing mechanism of novel carbon nanotube – Carbon fibre hybrid composites. Carbon N Y 2016;109:74–86. doi:10.1016/J.CARBON.2016.07.058.

[42] Li Q, Church JS, Naebe M, Fox BL. A systematic investigation into a novel method for preparing carbon fibre–carbon nanotube hybrid structures. Compos Part A Appl Sci Manuf 2016;90:174–85. doi:10.1016/J.COMPOSITESA.2016.05.004.

[43] Yamamoto N, Hart AJ, Garcia EJ, Wicks SS, Duong HM, Slocum AH, et al. High-yield growth and morphology control of aligned carbon nanotubes on ceramic fibers for multifunctional enhancement of structural composites. Carbon N Y 2009;47:551–60.

[44] Zhao Z-G, Ci L-J, Cheng H-M, Bai J-B. The growth of multi-walled carbon nanotubes with different morphologies on carbon fibers. Carbon N Y 2005;43:663–5.

[45] Thostenson ET, Li WZ, Wang DZ, Ren ZF, Chou TW. Carbon nanotube/carbon fiber hybrid multiscale composites. J Appl Phys 2002;91:6034–7. doi:10.1063/1.1466880.

[46] Aziz S, Rashid SA, Rahmanian S, Salleh MA. Experimental evaluation of the interfacial properties of carbon nanotube coated carbon fiber reinforced hybrid composites. Polym Compos 2015;36:1941–50. doi:10.1002/pc.23103.

[47] Kalamkarov AL, Georgiades A V, Rokkam SK, Veedu VP, Ghasemi-Nejhad MN. Analytical and numerical techniques to predict carbon nanotubes properties. Int J Solids Struct 2006;43:6832–54.

[48] Li C, Chou T-W. A structural mechanics approach for the analysis of carbon nanotubes.

Int J Solids Struct 2003;40:2487–99.

[49] Odegard GM, Gates TS, Wise KE, Park C, Siochi EJ. Constitutive modeling of nanotube-reinforced polymer composites. Compos Sci Technol 2003. doi:10.1016/S0266-3538(03)00063-0.

[50] Rafiee R, Maleki Moghadam R. Simulation of impact and post-impact behavior of carbon nanotube reinforced polymer using multi-scale finite element modeling. Comput Mater Sci 2012;63:261–8. doi:10.1016/j.commatsci.2012.06.010.

[51] Hill R. A self-consistent mechanics of composite materials. J Mech Phys Solids 1965;13:213–22. doi:10.1016/0022-5096(65)90010-4.

[52] Yas MH, Heshmati M. Dynamic analysis of functionally graded nanocomposite beams reinforced by randomly oriented carbon nanotube under the action of moving load. Appl Math Model 2012;36:1371–94. doi:10.1016/J.APM.2011.08.037.

[53] Kulkarni M, Carnahan D, Kulkarni K, Qian D, Abot JL. Elastic response of a carbon nanotube fiber reinforced polymeric composite: a numerical and experimental study. Compos Part B Eng 2010;41:414–21.

[54] Shokrieh MM, Rafiee R. Prediction of mechanical properties of an embedded carbon nanotube in polymer matrix based on developing an equivalent long fiber. Mech Res Commun 2010;37:235–40. doi:10.1016/J.MECHRESCOM.2009.12.002.

[55] Tucker III CL, Liang E. Stiffness predictions for unidirectional short-fiber composites: Review and evaluation. Compos Sci Technol 1999;59:655–71.

[56] Mathilde Barral, George Chatzigeorgiou, Fodil Meraghni, Renan Léon, Homogenization using modified Mori-Tanaka and TFA framework for elastoplastic-viscoelastic-viscoplastic composites: Theory and numerical validation, International Journal of Plasticity, Volume 127, 2020, 102632, https://doi.org/10.1016/j.ijplas.2019.11.011.

[57] Mori T, Tanaka K. Average stress in matrix and average elastic energy of materials with misfitting inclusions. Acta Metall 1973. doi:10.1016/0001-6160(73)90064-3.

[58] Wang J, Pyrz R. Prediction of the overall moduli of layered silicate-reinforced

nanocomposites-part I: Basic theory and formulas. Compos Sci Technol 2004. doi:10.1016/S0266-3538(03)00024-1.

[59] Lu P, Leong YW, Pallathadka PK, He CB. Effective moduli of nanoparticle reinforced composites considering interphase effect by extended double-inclusion model–Theory and explicit expressions. Int J Eng Sci 2013;73:33–55.

[60] Chen T, Dvorak GJ, Benveniste Y. Mori-Tanaka estimates of the overall elastic moduli of certain composite materials. J Appl Mech 1992;59:539–46.

[61] Shi D-L, Feng X-Q, Huang YY, Hwang K-C, Gao H. The Effect of Nanotube Waviness and Agglomeration on the Elastic Property of Carbon Nanotube-Reinforced Composites. J Eng Mater Technol 2004;126:250–7. doi:10.1115/1.1751182.

[62] Eshelby JD. The determination of the elastic field of an ellipsoidal inclusion, and related problems. Proc R Soc London Ser A Math Phys Sci 1957;241:376–96.

[63] Mura T. Micromechanics of defects in solids. Springer Science & Business Media; 2013.

[64] Reddy JN. Mechanics of laminated composite plates and shells: theory and analysis. CRC press; 2003.

[65] Ferrari M, Johnson GC. Effective elasticities of short-fiber composites with arbitrary orientation distribution. Mech Mater 1989;8:67–73. doi:10.1016/0167-6636(89)90006-9.

[66] Marom G, Weinberg A. The effect of the fibre critical length on the thermal expansion of composite materials. J Mater Sci 1975;10:1005–10.

[67] Bert CW, Kline RA. Composite-material mechanics: Properties of planar-random fiber composites. Polym Compos 1985;6:133–41.

[68] Alamusi, Hu N, Jia B, Arai M, Yan C, Li J, et al. Prediction of thermal expansion properties of carbon nanotubes using molecular dynamics simulations. Comput Mater Sci 2012;54:249–54. doi:10.1016/J.COMMATSCI.2011.10.015.

[69] Ugural AC, Fenster SK. Advanced strength and applied elasticity. Pearson education; 2003.

[70] Quek MY, Yue CY. Axisymmetric stress distribution in the single filament pull-out test.

Mater Sci Eng A 1994;189:105–16.

[71] Song D-Y, Takeda N, Ogihara S. A method of stress analysis for interfacial property evaluation in thermoplastic composites. Mater Sci Eng A 2000;278:242–6.

[72] Miyagawa H, Mase T, Sato C, Drown E, Drzal LT, Ikegami K. Comparison of experimental and theoretical transverse elastic modulus of carbon fibers. Carbon N Y 2006;44:2002–8.

[73] Dutton S, Kelly D, Baker A. Composite materials for aircraft structures. American Institute of Aeronautics and Astronautics; 2004.

[74] Sager RJ, Klein PJ, Lagoudas DC, Zhang Q, Liu J, Dai L, et al. Effect of carbon nanotubes on the interfacial shear strength of T650 carbon fiber in an epoxy matrix. Compos Sci Technol 2009;69:898–904.

[75] Zhao Z, Teng K, Li N, Li X, Xu Z, Chen L, et al. Mechanical, thermal and interfacial performances of carbon fiber reinforced composites flavored by carbon nanotube in matrix/interface. Compos Struct 2017;159:761–72.

[76] Chen, L., Jin, H., Xu, Z., Li, J., Guo, Q., Shan, M., Yang, C., Wang, Z., Mai, W., & Cheng, B. (2015). Role of a gradient interface layer in interfacial enhancement of carbon fiber/epoxy hierarchical composites. Journal of Materials Science, 50(1), 112–121.

[77] Ren X, Burton J, Seidel GD, Lafdi K. Computational multiscale modeling and characterization of piezoresistivity in fuzzy fiber reinforced polymer composites. Int J Solids Struct 2015;54:121–34.

[78] Shazed MA, Suraya AR, Rahmanian S, Mohd Salleh MA. Effect of fibre coating and geometry on the tensile properties of hybrid carbon nanotube coated carbon fibre reinforced composite. Mater Des 2014;54:660–9. doi:10.1016/J.MATDES.2013.08.063.

[79] Deng C, Jiang J, Liu F, Fang L, Wang J, Li D, et al. Influence of graphene oxide coatings on carbon fiber by ultrasonically assisted electrophoretic deposition on its composite interfacial property. Surf Coatings Technol 2015;272:176–81.